PROTEINS
STRUCTURE ■ FUNCTION ■ BIOINFORMATICS

Atomistic mechanisms of huntingtin N-terminal fragment insertion on a phospholipid bilayer revealed by molecular dynamics simulations

Sébastien Côté,[1]* Guanghong Wei,[2] and Normand Mousseau[1]

[1] Département de Physique and Groupe de recherche sur les protéines membranaires (GEPROM), Université de Montréal, Montréal (Québec), Canada

[2] State Key Laboratory of Surface Physics and Department of Physics, Fudan University, Shanghai, 200433, China

ABSTRACT

The huntingtin protein is characterized by a segment of consecutive glutamines (Q_N) that is responsible for its fibrillation. As with other amyloid proteins, misfolding of huntingtin is related to Huntington's disease through pathways that can involve interactions with phospholipid membranes. Experimental results suggest that the N-terminal 17-amino-acid sequence (htt^{NT}) positioned just before the Q_N region is important for the binding of huntingtin to membranes. Through all-atom explicit solvent molecular dynamics simulations, we unveil the structure and dynamics of the $htt^{NT}Q_N$ fragment on a phospholipid membrane at the atomic level. We observe that the insertion dynamics of this peptide can be described by four main steps—approach, reorganization, anchoring, and insertion—that are very diverse at the atomic level. On the membrane, the htt^{NT} peptide forms a stable α-helix essentially parallel to the membrane with its nonpolar side-chains—mainly Leu-4, Leu-7, Phe-11 and Leu-14—positioned in the hydrophobic core of the membrane. Salt-bridges involving Glu-5, Glu-12, Lys-6, and Lys-15, as well as hydrogen bonds involving Thr-3 and Ser-13 with the phospholipids also stabilize the structure and orientation of the htt^{NT} peptide. These observations do not significantly change upon adding the Q_N region whose role is rather to provide, through its hydrogen bonds with the phospholipids' head group, a stable scaffold facilitating the partitioning of the htt^{NT} region in the membrane. Moreover, by staying accessible to the solvent, the amyloidogenic Q_N region could also play a key role for the oligomerization of $htt^{NT}Q_N$ on phospholipid membranes.

Proteins 2014; 82:1409–1427.

Key words: Huntingtin protein; Huntington's disease; httNTQN monomer; peptide–membrane interactions; all-atom explicit solvent simulations.

INTRODUCTION

The huntingtin protein belongs to a family of 10 proteins that are related to trinucleotide CAG/polyglutamine repeats disorder.[1–3] These proteins are characterized by a consecutive segment of glutamines of varying lengths that can lead, when the number of repeats exceeds a given threshold, to misfolding and fibrillation. Misfolding of huntingtin is related to the Huntington's disease and it occurs when its consecutive segment of glutamines reaches 35, with the neurotoxicity strength likely being correlated to this length.[4] The origin of the neurotoxicity is still under debate, but experimental evidences suggest that it could involve nonphysiological interactions of huntingtin with membrane-containing organelles of the cell,[5–9] a characteristic shared by many other neurodegenerative diseases.[10,11] Most experiments and simulations focus on huntingtin exon 1 or some of its fragments since these are sufficient to induce a pathology *in vivo* similar to the full-length protein.[12–14] Huntingtin exon 1 consists of a 17-residues amphipathic N-terminal

Additional Supporting Information may be found in the online version of this article.

Grant sponsors: Canada Research Chairs program, the Fonds québécois de recherche sur la nature et les technologies (FQRNT), the Natural Sciences and Engineering Research Council of Canada (NSERC), the Fonds de recherche en santé du Québec (FRSQ), and National Natural Science Foundation (NSF) of China (Grant No. 11074047).

*Correspondence to: Normand Mousseau, Département de Physique and Groupe de recherche sur les protéines membranaires (GEPROM), Université de Montréal, C.P. 6128, succursale Centre-ville, Montréal (Québec), Canada.
E-mail: normand.mousseau@umontreal.ca

Received 25 September 2013; Revised 27 December 2013; Accepted 6 January 2014
Published online 10 January 2014 in Wiley Online Library (wileyonlinelibrary.com). DOI: 10.1002/prot.24509

(htt^{NT}), a consecutive segment of glutamines (Q_N), a consecutive segment of prolines (P_N) and a proline-rich segment.

As other amyloid proteins, huntingtin can aggregate into fibrils through a nucleation-dependent process.[15–18] Its kinetics of aggregation is dependent on the number of glutamines[19] as well as on the presence of the neighboring segments[20,21] such as htt^{NT} and P_N. For instance, the nucleus size of Q_N is reduced from 4 to 1 when the number of glutamines passes from 23 to 26,[22] while the presence of the htt^{NT} segment leads to a negative nucleus size suggesting spontaneous fibrillation[23] or limitations of the homogenous nucleation model.[24] The aggregation kinetics is also sequence-dependent since fibrillation is faster when the number of glutamines in the Q_N region increases[19,25] and when the htt^{NT} region is present,[23,26] while the fibrillation kinetics is slowed down by the presence of the P_N region.[27,28]

Since it is difficult to resolve directly the atomic structures of huntingtin's transient monomer and small oligomers in solution due to fast aggregation, most structural information comes from solution circular dichroism (CD) experiments. These measures show that the htt^{NT} peptide in solution populates a distribution of α-helical content that varies from 10 to 55%.[8,23,29,30] Nuclear magnetic resonance measurements on the structural ensemble of the htt^{NT} peptide suggest, for their part, that it does not form stable α-helices.[23] X-rays scattering on a fusion protein of maltose-binding protein and the exon 1 of huntingtin (MBP-$htt^{NT}Q_{17}$-ex1) shows that the htt^{NT} segment folds into an α-helix, while the Q_N segment appears to be unstructured[31] as also shown by fluorescence correlation spectroscopy.[32]

Computational studies have partially complemented these experiments by investigating the structures and folding dynamics of monomer/oligomers at the atomic level. For instance, simulations on the monomeric and dimeric Q_N peptides of various lengths revealed that they form mostly disordered, collapsed globules suggesting that the formation of β-sheets is more favorable in aggregates of higher molecular weights.[33,34] The Q_N peptide can nevertheless also adopt various stable motifs at the monomer level such as α-helix, β-sheet and β-sheetstack[35] as well as β-helix.[36,37] Moreover, the β-sheet stability increases as Q_N is longer[38–41] and as the oligomeric weight increases.[39,42,43] Other simulations were performed to discriminate the widely different repeat motifs suggested for the fibril morphologies of Q_N.[44–46] The effect of neighboring regions on Q_N folding has also been investigated. For instance, simulations on htt^{NT}47,48 and $htt^{NT}Q_NP_{11}$[49] monomers showed that the htt^{NT} region can populate alpha-helical configurations, while others suggest a rather amorphous monomer and dimer for $htt^{NT}Q_N$.[30] The htt^{NT} region stabilizes β-sheet structures in the Q_N region of small oligomers of $htt^{NT}Q_N$,[43] while the P_N region, for its part, reduces the β-sheet probability of the Q_N region in the exon 1 of huntingtin.[40] Overall, combining experiments and simulations helped to understand the structural changes occurring in $htt^{NT}Q_N$ during its aggregation without yet leading to a consensual family of conformations.

As well as being an important modulator of the aggregation in solution, both the presence of the htt^{NT} region and the number of glutamines in the Q_N region also modulate the interactions of huntingtin with phospholipid membranes. In the cell, the htt^{NT} region of huntingtin strongly influences its localization on the mitochondria, endoplasmic reticulum and Golgi.[8,9] Interestingly, htt^{NT}s amino acids sequence shares similarities with signaling peptides as it is amphipathic and it displays, when mapped to the α-helix topology, an amphipathic plane separating on opposite sides its nonpolar from its charged amino acids. It could therefore play a key part in huntingtin's physiological roles by controlling its localization in the cell. The length of Q_N also modulates the localization of huntingtin by increasing the nuclear entry[50,51] leading, when above the pathological threshold, to deleterious effects on the cell through various nuclear and extra-nuclear pathways many of which involve membrane-containing structures.[52] In vitro experiments further suggest that these pathways could involve interactions with membrane as $htt^{NT}Q_N$ disrupts DMPC:POPE (1:1) vesicles in a Q_N-length dependent manner as shown by differential scanning calorimetry experiments.[53] Similar observations were also obtained from atomic force microscopy (AFM) experiments on supported lipid membranes from brain extracts.[54] Moreover, htt^{NT} alone can cause membrane permeation of large unilamellar vesicles as shown by calcein release assays.[29] Finally, the lipid composition also modulates these interactions as huntingtin binds more strongly in the presence of higher ratios of POPE or PI phospholipids.[55,56] Overall, these observations indicate that the interactions of huntingtin with lipid membranes might be related to its physiological and pathological roles raising the need to precisely characterize these interactions at the atomic level.

In this article, we develop an atomistic picture of the partitioning dynamics of $htt^{NT}Q_N$ in a phospholipid membrane through all-atom, explicit solvent molecular dynamics (MD) simulations. This study is inspired by other computational simulations that have helped characterize the structures and dynamics of the membrane interactions of other well-known amyloid proteins such as amyloid-beta (Aβ)[57,58] and islet amyloid polypeptide (IAPP).[59,60] More precisely, the main goals of this study are to unveil the insertion dynamics of htt^{NT} on a phospholipid bilayer and to describe the impact of the Q_N region. Moreover, we determine the key amino acids, through their interactions with the phospholipid membrane, at the origin of $htt^{NT}Q_N$ structural stability and orientation using a detailed residue-level analysis

Table I
Summary of the performed simulations

Simulations	Time (ns)	Initial conf.	Box size (nm)	No. H_2O	No. POPE
168–POPE–hexa	350	–	$a=b=7.3, c=8.6$	6 692	168
240–POPE–hexa	350	–	$a=b=8.8, c=8.6$	9 793	240
328–POPE–hexa	350	–	$a=b=10.4, c=8.5$	13 328	328
sol–httNT	650 × 2	α	$a=b=c=8.1$	13 284	0
AMBER99sb*-ILDN					
sol–httNT	500 × 2	α	$a=b=c=8.1$	13 284	0
OPLS-AA					
sol–httNT	500 × 2	α	$a=b=c=8.1$	13 284	0
CHARMM27					
sol–httNT	500 × 2	α	$a=b=c=8.1$	13 284	0
AMBER03					
httNT_α	500 × 5	α	$a=b=7.4, c=11.0$	10 613	168
httNT_coil	500	coil	$a=b=7.4, c=10.1$	9 384	168
httNT_α–ins	500 × 2	Inserted α	$a=b=7.4, c=9.0$	7479	164
httNTQ20_α	500 × 5	A	$a=b=10.3, c=12.4$	24 466	328
httNTQ20_coil	500	Coil	$a=b=10.3, c=11.5$	21 930	328
httNTQ20_α–ins	500 × 2	Inserted α	$a=b=10.3, c=9.3$	15 952	318
httNTQ20_α-coil–ins	500	Inserted α-coil	$a=b=10.4, c=9.2$	15 952	318
httNTQ10_α	500 × 2	α	$a=b=8.8, c=11.1$	15 462	240
httNTQ10_coil	500	Coil	$a=b=8.8, c=11.2$	15 697	240

The box size corresponds to the initial length of the principal axes which are subject to small variation during the simulations as they are done in the NPT ensemble. The periodic boxes are either an octahedron ($\alpha=70.5^\circ, \beta=109.5^\circ, \gamma=70.5^\circ$) for the simulations in solution or hexagonal prism ($\alpha=90^\circ, \beta=90^\circ, \gamma=120^\circ$) for the simulations with a phospholipid membrane. All simulations are done using the AMBER99sb*-ILDN forcefield for the protein unless otherwise specified.

combining insertion depth, solvent accessibility, hydrogen bond and salt-bridge measurements. This information is of outmost importance as it complements previous experimental studies on htt$^{NT}Q_N$—membrane systems for which such a level of atomic precision is missing.

Our paper is constructed as follows. We first describe the simulation parameters used, the choice of protein and phospholipid forcefields, the preparation of the initial configurations, and the analysis protocol. We next present our results on the interactions of the htt^{NT} and htt$^{NT}Q_{20}$ fragments with a phospholipid bilayer. Finally, we relate our results to previous experiments and discuss their implications for the huntingtin protein.

MATERIALS AND METHODS

We investigate the atomistic origin of adsorption, insertion and stability of huntingtin N-terminal (htt$^{NT}Q_N$) on a phospholipid membrane composed of 1-palmitoyl-2-oleoyl-sn-glycero-3-phosphoethanolamine (POPE) phospholipids using all-atom, explicit solvent molecular dynamics simulations. We also investigate the effect of the number of glutamines in Q_N by simulating fragments counting 0, 10, and 20 glutamines, with more emphasis on 0 and 20. The amino sequence of htt$^{NT}Q_N$ is MATLEKLMKAFESLKSFQ$_N$-NME with the subscript N referring to the number of glutamines. Since this sequence is present at the N-terminal of the longer huntingtin sequence, we N-methylated its C-terminal in order to remove the carboxylate's negative charge which could otherwise impact our results. In the current study, we choose POPE phospholipids since experiments show that the aggregation of the huntingtin N-terminal is modulated by the number of glutamines for membrane containing higher ratios of this phospholipid.[56] Moreover, experiments show that htt$^{NT}Q_N$ perturbs the physical properties of DMPC:POPE (50:50*M* ratio) membranes.[53] Finally, we choose to construct our membranes using a single phospholipid species as we want to uncouple the effect of POPE from other phospholipids.

All simulations, which are summarized in Table I, are performed for at least 500 ns for a total simulation time of 15.4 μs. The simulations parameters as well as the preparation protocol for the initial configurations are described next.

MD simulations

All molecular dynamics (MD) simulations are performed with the software GROMACS version 4.5.4.[61–64] Simulations are done in the NPT ensemble using the AMBER99sb*-ILDN forcefield for the protein parameters[65–68] and the Stockholm lipids (SLIPIDS) forcefield for the phospholipid parameters[69–72] as justified below. We use the same simulation parameters and water model (TIP3P) as in the original SLIPIDS paper.[70] The temperature is set at 303 K using the Nosé-Hoover thermostat[73,74] with a coupling constant of 0.5 ps. The pressure is semi-isotropically set at 1.013 bar using the Parrinello-Rahman barostat[75,76] with a coupling constant of 10 ps. Lennard-Jones energy is switched to zero from 1.4 nm to 1.5 nm. Electrostatic interactions are

treated by Particle-Mesh-Ewald (PME)[77,78] with a real space cut-off of 1.4 nm. Bond lengths are constrained using LINCS[79] and water geometry with SETTLE[80] allowing an integration time step of 2 fs. The center of mass linear momentum is removed every 20 fs. Unless otherwise stated, all these parameters are also used to prepare and equilibrate the initial configurations of the protein, membrane and protein-membrane systems.

Membranes are prepared as follow. We build membranes of 1-palmitoyl-2-oleoyl-sn-glycero-3-phosphoethanolamine (POPE) with a hexagonal cross-section from the original 128 POPE rectangular membrane presented in the original SLIPIDS paper[70] (http://people.su.se/~jjm/). Three different sizes of hexagonal membranes are created: 168 phospholipids for htt^{NT}, 240 phospholipids for $htt^{NT}Q_{10}$, and 328 phospholipids for $htt^{NT}Q_{20}$. Each system size is chosen such that the distances between the peptide and its periodic images are always greater than 3.0 nm during all simulations. Each membrane is then equilibrated for 350 ns. The areas per lipid averaged over the last 100 ns are 0.563 ± 0.009 nm^2 (168–POPE–hexa), 0.562 ± 0.007 nm^2 (240–POPE–hexa), and 0.559 ± 0.007 nm^2 (328–POPE–hexa), in agreement with the *in silico* value of 0.562 ± 0.004 nm^2 obtained in the original SLIPIDS paper[70] and with the experimental value[81] of 0.566 nm^2. The order parameters of the acyl chains averaged over the last 100 ns also agree with the original SLIPIDS paper[70] as shown in Supporting Information Figure S1.

Using the equilibrated membranes, the initial protein-membrane systems are prepared as follows. Two different initial configurations are used for each peptide: a single α-helix and a single random coil (Supporting Information Fig. S2). The random coil configuration is generated from a 10-ns MD simulation in solution starting from a completely extended structure. For both initial configurations, the protein center of mass is placed at 4.5 nm from the membrane center-of-mass, and the principal axis of the backbone atoms is aligned parallel to the membrane such that the initial minimum distance between the protein and the membrane is greater than 2.0 nm, that is the protein is at least 0.5 nm beyond real space cutoffs from the membrane. Finally, the box is filled with water molecules and two chloride ions are added to neutralize each system. A preinserted α-helix is also used as initial configuration for htt^{NT} and $htt^{NT}Q_{20}$ (Supporting Information Fig. S2). Using InflateGRO2,[82] the peptide is inserted such that the principal axis of its backbone atoms is aligned parallel to the membrane surface and that its nonpolar residues are pointing toward the hydrophobic core of the membrane. For $htt^{NT}Q_{20}$, a configuration with an α-helical htt^{NT} region and a random coiled Q_N region is also used. This initial state is obtained from a 10-ns MD simulation starting from the pre-inserted and equilibrated single α-helix configuration during which the heavy atoms of the htt^{NT} region are harmonically restrained to their initial position and the ψ dihedral angles of one each two residues in the Q_N region are restrained harmonically to 135°. These restrains allow to keep the htt^{NT} region folded into an α-helix as well as disordering the Q_N region during the preparation of this initial state.

Before each MD simulation, we equilibrate the initial configuration by first minimizing the energy using the conjugate gradient algorithm with a steepest descent step applied once every 100 steps, and by secondly equilibrating the system for 1 ns using a 1 fs time step and restrains on all heavy atoms of the protein. The 0 ns configuration in all figures refers to the structures obtained after these pre-MD steps.

Forcefield

The forcefield selection is motivated by several aspects, the most important of which is that the protein forcefield correctly samples the equilibrium secondary structure of huntingtin 17-amino-acid N-terminal (htt^{NT}) positioned just before the consecutive segment of glutamines (Q_N). Circular dichroism (CD) spectroscopy studies show that the htt^{NT} peptide samples some α-helical content in solution.[8,23,29,30] Nuclear magnetic resonance (NMR) studies further show that there is no stable α-helix in solution.[23] We evaluate different forcefields by simulating this peptide in solution using the simulation parameters previously presented. As described in the Supplementary Material, some popular protein forcefields either overestimate (CHARMM27[83,84] and AMBER03[85]) or underestimate (OPLS-AA\L[86,87]) the fraction of α-helices sampled by htt^{NT}. On the other hand, we found that AMBER99sb*-ILDN[65] has the least bias toward the fully formed alpha-helix or fully random-coil states, two ensembles that do not correspond to the aforementioned CD and NMR experimental results on the htt^{NT} peptide in solution. Moreover, this latter forcefield correctly reproduces the folding and stability of diverse proteins as shown by microsecond time scale MD simulations.[88–91] Therefore, for our simulations, we select the forcefield AMBER99sb*-ILDN which originates from the combination of two corrections to AMBER99sb:[68] AMBER99sb-ILDN that corrects the energy landscape of the χ_1 and χ_2 torsion angles of the isoleucine, leucine, aspartate and asparagine residues,[66] and AMBER99sb* that corrects the α-helix–coil imbalance impacting the conformational sampling.[67]

Once we determined that AMBER99sb*-ILDN best matches the structural ensemble of the htt^{NT} peptide in solution, we choose a phospholipid forcefield that is compatible with the AMBER forcefields family, usable in the NPT ensemble as well as good at reproducing diverse bilayer properties measured experimentally. As previously shown, the Stockholm lipids (SLIPIDS) satisfy these three conditions on time scales of hundreds of

nanoseconds for many phospholipids.[69–71,92] The combination SLIPIDS and AMBER has been used to compute the free energy of insertion of several compounds into phospholipid bilayers[92] and the tilt angle of the WALP23 peptide inserted in phospholipid bilayers.[70] The computed quantities are in good agreement with experimental measurements.[70,92]

Analysis

To characterize the htt$^{NT}Q_N$–membrane system, we compute several quantities using inhouse codes and GROMACS utilities, unless otherwise stated. To describe the backbone structure, the α-helix propensity is computed using STRIDE.[93] To quantify the degree of insertion, the center-of-mass distance between each residue of htt$^{NT}Q_N$ and the membrane, as well as the solvent accessible surface area using a water probe radius of 1.4 Å[94] are computed. To quantify the membrane properties, the order parameters of the acyl chains are computed using the order program of the MDynaMix software.[95] To quantify the peptide–membrane interactions, salt-bridges are considered when two oppositely charged groups are within 4 Å of each other,[96] and hydrogen bonds are considered when the donor–acceptor distance is smaller than 3.5 Å and the hydrogen–donor–acceptor angle is smaller than 30°. To cluster the configurations, the root mean square distance (RMSD) between the backbone atoms is first computed on any pair of configurations which are then regrouped into clusters from the largest to the smallest by removing the clustered configurations each time a new cluster is found. The clusters have the following properties: their center has a backbone RMSD of at most 2.0 Å against all other configurations inside the cluster and a given configuration can not be found in two different clusters. All figures showing the time-evolution of some quantity display the running time average of the data using 5-ns time windows. All reported error bars on averaged quantities correspond to one statistical standard deviation. Finally, molecular graphics images are generated using the PyMOL software (http://www.pymol.org).

RESULTS

htt^{NT} with a bilayer

To investigate the insertion dynamics of htt^{NT} alone, we launch five independent MD simulations starting from the same initial configuration with different initial velocity distributions (Table I). We choose to start with a single α-helix state for two main reasons: (1) htt^{NT} samples widely different α-helical configurations in solution with relatively similar weights (Supporting Information Figs. S3 and S4), so choosing a specific one over another might induce a bias and (2) the atomic structure of htt^{NT} alone in solution has not yet been resolved by NMR or X-rays crystallography. As shown below, this particular choice does not seem to bias our results since similar results are obtained when a random coil configuration is taken for the initial state.

Three trajectories show partial insertion of the nonpolar residues of the htt^{NT} peptide and they are displayed in Figure 1 (simulations httNT_α_1 and httNT_α_2) and Supporting Information Figure S5 (simulation httNT_α_3). These are characterized by four main steps: (1) an approach step that seems to be driven by long-range electrostatic interactions between the peptide and the phospholipids' head group, (2) a reorganization step during which the peptide undergoes structural changes in order to bring the nonpolar residues nearer to the membrane core, (3) an anchoring step initialized by the positioning of a nonpolar residue such as the phenylalanines inside the hydrophobic core of the membrane, and (4) an insertion step during which the other nonpolar residues are partitioned in the membrane as structural reorganization continues. Because of the large accessible configurational space, considerable differences occur in the details of each step. These differences are summarized in Table II which shows, in order of occurrence, the residues forming their first contact with the bilayer for the approach step as well as those found below the phosphate groups of the bilayer for the anchoring and insertion steps. First, the approach step seems to be initiated by different charged parts of the peptide: Lys-15 is within the first residues to come into contact with the membrane for the httNT_α_1 and httNT_α_3 trajectories, while it is the N-terminal for httNT_α_2. Second, structural reorganization can be quite different as the htt^{NT} peptide stays mostly α-helical in the first trajectory ($55 \pm 18\%$), while it becomes largely disordered in the second and third trajectories ($0 \pm 1\%$ and $2 \pm 8\%$, respectively) as shown in Figure 2. Third, the anchoring step can be initiated by a phenylalanine (Phe-17 for httNT_α_1 and Phe-11 for httNT_α_3) or by other nonpolar residues (Leu-7 for httNT_α_2). Fourth, the insertion step can occur in a different order of residues: Leu^7–Met^8–Leu^4–Met^1 for httNT_α_1, Met^8–Phe^{11}–Leu^{14}–Phe^{14} for httNT_α_2, and Leu^7–Met^8–Met^1–Leu^4 for httNT_α_3. Finally, the httNT_α_1 trajectory seems to have reached a metastable state with many inserted nonpolar residues (Fig. 3). For their part, the other two trajectories are less inserted and still undergo small structural changes as their nonpolar residues sample a wider range of positions from the bilayer's center.

The last two trajectories (simulations httNT_α_4 and httNT_α_5), for which the peptide does not insert and remains trapped between the third and fourth steps, are shown in Supporting Information Figure S5. Looking more closely, the peptide's attempts to bring its nonpolar residues toward the hydrophobic core of the membrane are unsuccessful because it needs to undergo structural

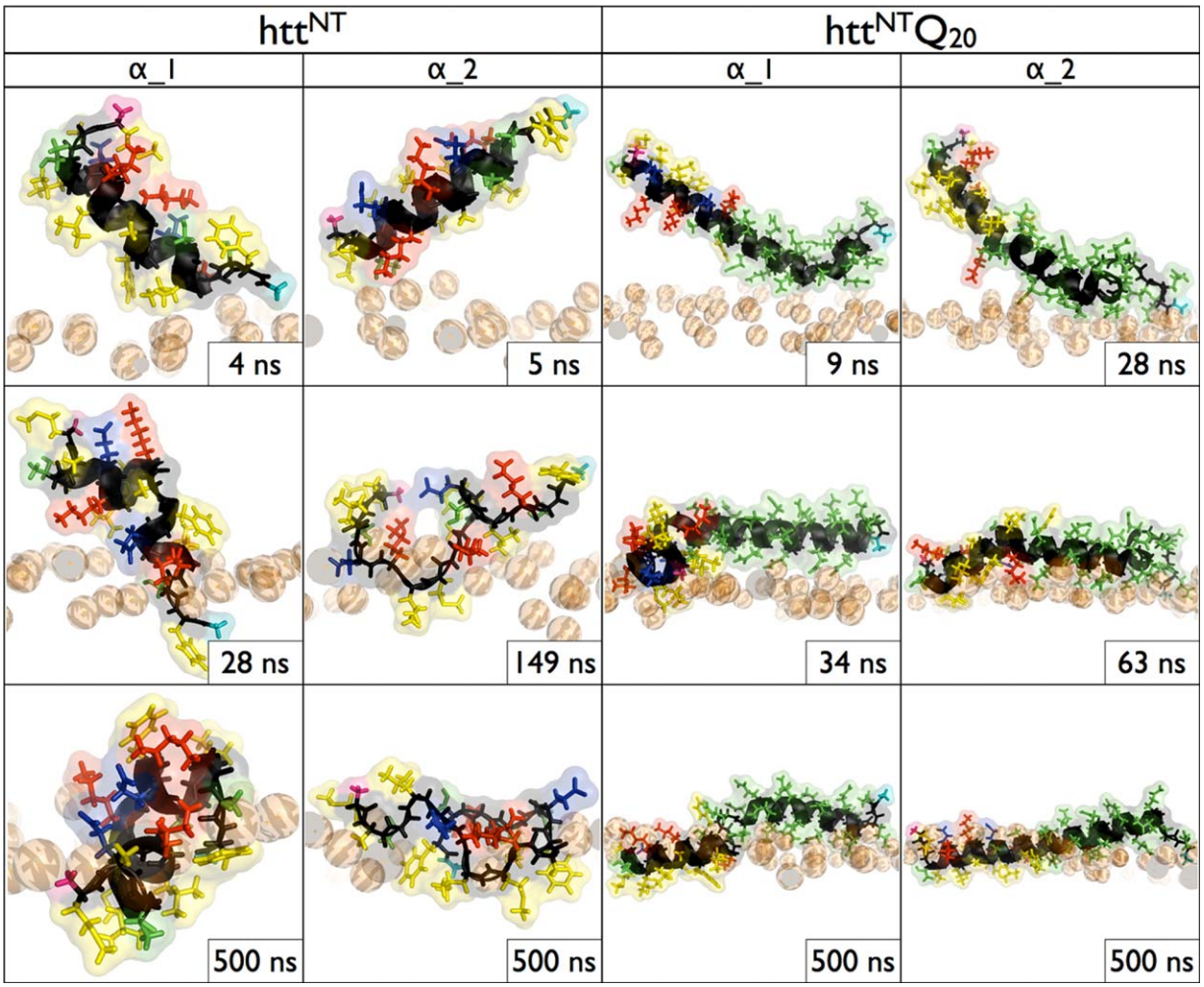

Figure 1

The httNT_α_1 and httNT_α_2 trajectories for htt^{NT} are shown on the first and second columns, respectively. The httNTQ20_α_1 and httNTQ20_α_2 trajectories for htt^{NT}Q$_{20}$ are shown on the third and fourth columns, respectively. The nonpolar, negatively charged, positively charged and polar amino acids of the peptide are respectively shown in yellow, red, blue and green. The backbone atoms are displayed in black, and the N- and C-terminal are respectively shown in pink and teal. Only the phosphorus atom is displayed as an orange sphere for each phospholipid. [Color figure can be viewed in the online issue, which is available at wileyonlinelibrary.com.]

changes that are impaired by strong electrostatic interactions between its charged residues and the phospholipids' head group (Supporting Information Fig. S6). As a result, these trajectories are significantly less inserted and still undergo structural reorganizations (Supporting Information Fig. S7 vs. Fig. 3). Interestingly, these results suggest that the amount of α-helical content does not automatically correlate with a faster insertion of the nonpolar residues as these two trajectories, which do not insert, have a higher α-helical propensity than the httNT_α_2 and httNT_α_3 trajectories that insert (Table II). It is expected, however, from the htt^{NT}'s sequence, that insertion of all nonpolar residues requires the peptide to be in an α-helix.

We also investigate the insertion dynamics of htt^{NT} starting from a random coil that is not interacting with the membrane. Partial insertion of the nonpolar residues is observed in that trajectory which follows the same four main steps observed for the trajectories obtained when starting from a single α-helix conformation (Table II and Supporting Information Fig. S5, simulation httNT_coil). The approach and anchoring steps are respectively initialized by the N-terminal and Phe-17, and the α-helical content of the peptide does not increase significantly during the simulation. This further confirms that a significant α-helical propensity is not a necessary condition for a partial insertion of the nonpolar residues of htt^{NT} into the membrane. Further reorganization would, of course, be expected to occur if given enough time.

Overall, the completion of the four steps can span very different time scales from a several tenths to hundreds of nanoseconds and beyond our computational capacity. A

Table II
Insertion steps for all simulations done on httNT, httNTQ10 and httNTQ20

Simulations	Approach step	Anchoring step	Insertion step	Average α-helix (%)
httNT_α_1	Phe^{17} Lys^{15} Ser^{16} Leu^{14} Phe^{11}	Phe^{17}	Leu^{7} Met^{8} Leu^{4} Met^{1}	55 ± 18
httNT_α_2	Met^{1} Leu^{4} Ala^{2} Glu^{5} Met^{8} Thr^{3}	Leu^{7}	Met^{8} Phe^{11} Leu^{14} Phe^{17}	0 ± 1
httNT_α_3	Phe ^{17} Phe^{11} Lys^{15} Ser^{16} Met^{8} Leu^{4}	Phe^{11}	Leu^{7} Met^{8} Met^{1} Leu^{4}	2 ± 8
httNT_α_4	Phe ^{17} Lys^{15} Ser^{16} Phe^{11} Met^{8} Glu^{12}	Phe^{17}	–	58 ± 22
httNT_α_5	Glu ^{12} Lys^{15} Ser^{16} Ser^{13} Ala^{10} Phe^{17}	Phe^{17}	–	34 ± 16
httNT_coil	Met ^{1} Ala^{2} Leu^{4}	Leu^{4}	Phe^{17}	7 ± 12
httNT_α–ins_1	–	–	–	76 ± 15
httNT_α–ins_2	–	–	–	83 ± 8
httNTQ20_α_1	Q_N Lys^{9} Lys^{6}	Leu^{4}	Met^{1} Met^{8} Phe^{11} Leu^{7} Leu^{14}	72 ± 8
httNTQ20_α_2	Q_N Phe^{17}	Leu^{4}	Met^{8} Leu^{7} Phe^{11} Leu^{14} Phe^{17}	76 ± 11
httNTQ20_α_3	Q_N	–	–	64 ± 3
httNTQ20_α_4	Q_N Lys^{9}	Met^{1}	–	31 ± 21
httNTQ20_α_5	Q_N	–	–	80 ± 9
httNTQ20_coil	Q_N	–	–	2 ± 7
httNTQ20_α–ins_1	–	–	–	84 ± 8
httNTQ20_α–ins_2	–	–	–	81 ± 7
httNTQ20_α-coil–ins	–	–	–	74 ± 13
httNTQ10_α_1	Q_N	Met^{1}	–	42 ± 13
httNTQ10_α_2	Q_N	–	–	0 ± 4
httNTQ10_coil	Q_N	–	—	8 ± 13

The second column (approach step) displays the amino acids that contact the phospholipid membrane within 1 ns after the occurrence of the first contact. The third column (anchoring step) indicates the first nonpolar amino acid to be inserted in the membrane. The fourth column (insertion step) shows the nonpolar amino acids that partition in the membrane in order of occurrence for those that stay inserted up to the end of the simulation. The last two columns respectively displays the average α-helix propensity only on the htt^{NT} region over the last 200 ns. For the initially inserted peptide trajectories, the average is taken over the last 300 ns.

bottleneck seems to be particularly difficult to overcome using standard MD simulations on the sub-microsecond time scale. Insertion of all nonpolar residues requires important structural changes that can be impaired by the strong electrostatic interactions between the charged residues of the peptide and the phospholipids' head group as these must be temporarily broken in order to reach a more inserted state. As a result, large fluctuations occur in the Coulomb energy between the peptide and membrane, while the Lennard-Jones energy undergoes significantly smaller fluctuations (Supporting Information Fig. S6).

Having said that, it is nonetheless important to have an idea of what to expect for the final state of htt^{NT}. In order to address this, we investigate the stability of an initially inserted htt^{NT} starting from a well-structured single α-helix configuration (simulations httNT_α–ins_1 and httNT_α–ins_2) with initial tilt/rotational pitch angles of 86°/93°. Two independent 500 ns simulations, with different initial velocity distributions, show that the α-helical state is stable when the nonpolar residues of htt^{NT} are oriented toward the hydrophobic core of the membrane (Fig. 4). Over the last 300 ns, the α-helix is mainly parallel to the membrane with tilt/rotational pitch angles of 89 ± 8°/114 ± 11° (httNT_α–ins_1) and 89 ± 9°/100 ± 14° (httNT_α–ins_2) as shown in Table III. The α-helical propensities are 76 ± 15% (httNT_α–ins_1) and 83 ± 8% (httNT_α–ins_2) with a stable

Table III
Orientation of the amphipathic plane of the httNT region for simulations of both httNT and httNTQ20 starting from an initially inserted peptide, and all-atom RMSD with respect to the NMR model[97]

Simulation	Tilt angle (°)	Pitch angle (°)	RMSD (Å)
httNT_α–ins_1	89 ± 8	114 ± 11	2.3 ± 0.2
httNT_α–ins_2	89 ± 9	100 ± 14	2.3 ± 0.2
httNTQ20_α–ins_1	82 ± 8	107 ± 12	2.1 ± 0.1
httNTQ20_α–ins_2	84 ± 9	91 ± 14	2.2 ± 0.2
httNTQ20_α-coil–ins	83 ± 6	95 ± 12	2.4 ± 0.4
Experimental values	103 ± 5	137 ± 5	—

The tilt and rotational pitch angles are defined by the rotation of the amphipathic plane, initially in the z-x plane, around the negative *z*-axis (tilt) followed by the rotation around the new negative y-axis (rotational pitch) to its current orientation. The graphical definition of these angles along with the distributions of angles sampled during our simulations are shown in Supporting Information Figure S8. The experimental values have been taken from a NMR experimental study on the htt^{N}–bilayer system.[97] In our simulations, the initial values for the tilt/rotational pitch angles are 86°/93° (httNT_α–ins_1 and httNT_α–ins_2), 81°/124° (httNTQ20_α–ins_1 and httNTQ20_α–ins_2) and 82°/126° (httNTQ20_α-coil–ins). The all-atom RMSD is taken with respect to the structured segment (residues 5 to 17) of the NMR model. The averages are taken over the 200–500 ns time interval.

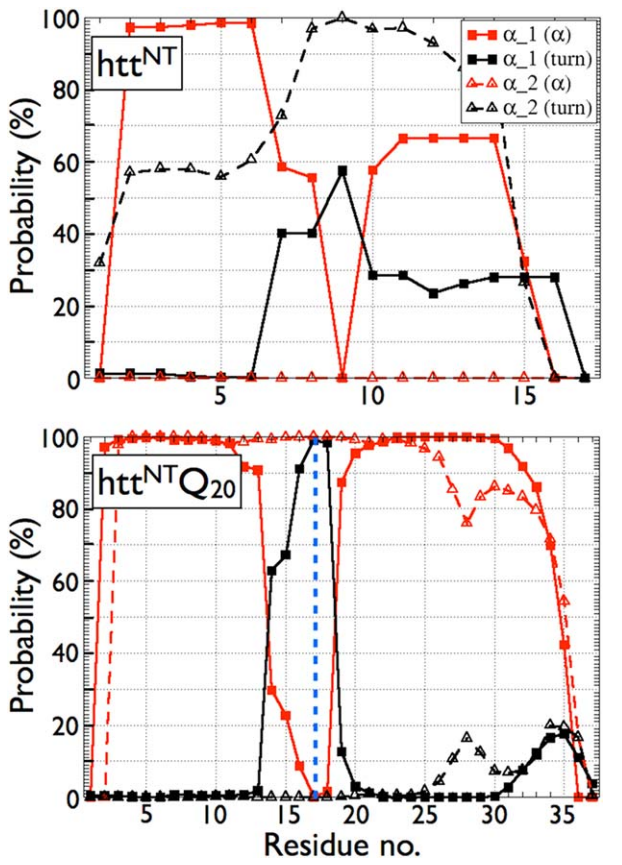

Figure 2

The per residue secondary structure propensities for the trajectories of htt^{NT} for httNT_α_1 and httNT_α_2 (top) and $htt^{NT}Q_{20}$ for httNTQ20_α_1 and httNTQ20_α_2 (bottom). The average propensities of α-helix and turn are respectively shown in red and black for the first (solid lines, solid squares) and the second trajectory (dotted lines, empty triangles). The average secondary structure is computed over the last 200 ns of the simulations. The vertical blue dotted line on the bottom panel indicates the last amino acid of the htt^{NT} region (Phe^{17}). [Color figure can be viewed in the online issue, which is available at wileyonlinelibrary.com.]

α-helix from Ala-2 to Ser-16 (Fig. 5). The structure and orientation of htt^{NT} are stabilized by key peptide–membrane interactions through salt-bridges involving Glu-5, Glu-12, Lys-6, and Lys-15, as well as hydrogen bonds involving Thr-3 and Ser-13 (Table IV). Nonpolar residues, mostly Leu-4, Leu-7, Phe-11, and Leu-14, are positioned away from the solvent in the hydrophobic core of the membrane (Fig. 6). We therefore expect that the htt^{NT} peptide in our previous simulations (Fig. 1 and Supporting Information Fig. S5) could undergo further structural reorganizations toward the stable α-helical configuration shown in Figure 4 given sufficient time.

$htt^{NT}Q_{20}$ with a bilayer

We now investigate the effect of the polyglutamine segment (Q_N) on the dynamics and equilibrium properties of the $htt^{NT}Q_N$ –phospholipid bilayer system. Five independent 500 ns molecular dynamics simulations each starting from the same initial structure with different initial velocity distributions were executed (Table I). As for the htt^{NT} peptide, the initial structure is a single α-helix since there is no high-resolution experimental structure of $htt^{NT}Q_N$ in solution at the moment. This choice does not seem to impact the sampling since very different trajectories are observed showing either insertion of almost all the nonpolar residues of the htt^{NT} region (for two trajectories) or no insertion at all (for three trajectories).

Analysis of the two trajectories characterized by the insertion of almost all the nonpolar residues (simulations httNTQ20_α_1 and httNTQ20_α_2) reveals that the four mains steps observed for the htt^{NT} peptide—approach, reorganization, anchoring and insertion—also describe the dynamics of insertion in the presence of the Q_N region (Fig. 1). It is in the details of each step that differences, mainly due to Q_N, are revealed as summarized in Table II. For instance, the lysines, as for the htt^{NT} peptide, but also the carbonyl and amine groups of the glutamines side-chain in the Q_N region can be within the first to interact with the membrane. Furthermore, during the reorganization step, the glutamines interact strongly with the phospholipids' head group through hydrogen bonds and the structural changes are less important than for htt^{NT} (Table II). More precisely, the largest structural changes are observed in the httNTQ20_α_1 trajectory between residues Leu-14 and Phe-17 that adopt a turn conformation linking the inserted α-helical htt^{NT} to the adsorbed Q_N (Fig. 2). By interacting strongly with the phospholipids' head group, the Q_N region then provides a stable scaffold for the partitioning of the nonpolar residues of the htt^{NT} region inside the hydrophobic core of the membrane. As a result, $htt^{NT}Q_{20}$ is more structured and more inserted than htt^{NT}. Over the last 200 ns, the position density of each nonpolar side-chain shows that the peptide has reached a metastable state with a more pronounced insertion than for the htt^{NT} peptide (Fig. 3).

The insertion of $htt^{NT}Q_{20}$ does not occur for the other three trajectories (simulations httNTQ20_α_3, httNTQ 20_α_4 and httNTQ20_α_5 displayed in Supporting Information Fig. S9) indicating that this process is not necessarily faster in the presence of Q_N. Similarly to htt^{NT}, these trajectories are trapped in the reorganization step (second step) due to the strong electrostatic interactions between the charged residues and the phospholipids' head group (Supporting Information Fig. S6). As a result, the nonpolar residues are trapped on the opposite side of the membrane and cannot be inserted in its hydrophobic core. Trajectories httNTQ20_α_3 and httNTQ20_α_5 undergo few structural changes during the last 200 ns as the positions of their nonpolar residues do not change much, while the position densities are broader in httNTQ20_α_4

Table IV
Per residue httNT–membrane interactions of httNT_α–ins_1 and httNT_α–ins_2

Simulations	Amino acids	Insertion depth (nm)	SASA (nm^2)	H-bonds (no.)	Salt-bridges (no.)
httNT_α–ins_1	htt^{NT}	1.9 ± 0.2	5.0 ± 0.9	3 ± 1 (98%)	2 ± 1 (80%)
	Met-1	1.6 ± 0.2	0.03 ± 0.06	–	–
	Ala-2	2.2 ± 0.2	0.4 ± 0.1	–	–
	Thr-3	1.7 ± 0.2	0.06 ± 0.07	1.0 ± 0.2 (72%)	–
	Leu-4	1.5 ± 0.2	0.01 ± 0.03	–	–
	Glu-5	2.2 ± 0.2	0.7 ± 0.3	1.1 ± 0.3 (30%)	1.0 ± 0.2 (31%)
	Lys-6	2.1 ± 0.2	0.7 ± 0.3	1.2 ± 0.5 (41%)	1.2 ± 0.4 (31%)
	Leu-7	1.4 ± 0.2	0.01 ± 0.02	–	–
	Met-8	1.8 ± 0.2	0.1 ± 0.1	–	–
	Lys-9	2.4 ± 0.2	1.1 ± 0.2	1.0 ± 0.2 (7%)	1.0 ± 0.2 (7%)
	Ala-10	1.8 ± 0.2	0.03 ± 0.04	–	–
	Phe-11	1.5 ± 0.2	0.01 ± 0.02	–	–
	Glu-12	2.2 ± 0.2	0.7 ± 0.2	1.0 ± 0.2 (39%)	1.1 ± 0.1 (40%)
	Ser-13	2.1 ± 0.2	0.2 ± 0.1	1.0 ± 0.1 (24%)	–
	Leu-14	1.5 ± 0.2	0.01 ± 0.02	–	–
	Lys-15	1.9 ± 0.2	0.3 ± 0.2	1.1 ± 0.4 (58%)	1.1 ± 0.3 (43%)
	Ser-16	2.2 ± 0.3	0.4 ± 0.1	1.0 ± 0.1 (11%)	–
	Phe-17	1.7 ± 0.3	0.1 ± 0.2	–	–
httNT_α–ins_2	htt^{NT}	1.9 ± 0.2	5.0 ± 0.8	3 ± 1 (100%)	2 ± 1 (84%)
	Met-1	1.7 ± 0.2	0.04 ± 0.07	–	–
	Ala-2	2.2 ± 0.2	0.3 ± 0.1	–	–
	Thr-3	1.7 ± 0.2	0.03 ± 0.05	1.0 ± 0.1 (89%)	–
	Leu-4	1.6 ± 0.2	0.01 ± 0.01	–	–
	Glu-5	2.3 ± 0.2	0.7 ± 0.2	1.0 ± 0.1 (35%)	1.0 ± 0.1 (36%)
	Lys-6	2.1 ± 0.2	0.6 ± 0.2	1.3 ± 0.5 (57%)	1.2 ± 0.4 (46%)
	Leu-7	1.5 ± 0.2	0.01 ± 0.01	–	–
	Met-8	2.0 ± 0.2	0.3 ± 0.1	–	–
	Lys-9	2.4 ± 0.2	1.1 ± 0.2	1.0 ± 0.2 (6%)	1.0 ± 0.1 (5%)
	Ala-10	1.7 ± 0.2	0.01 ± 0.02	–	–
	Phe-11	1.6 ± 0.2	0.02 ± 0.03	–	–
	Glu-12	2.3 ± 0.2	0.8 ± 0.2	1.2 ± 0.5 (17%)	1.1 ± 0.3 (18%)
	Ser-13	2.1 ± 0.2	0.2 ± 0.1	1.0 ± 0.1 (47%)	–
	Leu-14	1.5 ± 0.2	0.01 ± 0.01	–	–
	Lys-15	1.9 ± 0.2	0.3 ± 0.2	1.2 ± 0.4 (57%)	1.1 ± 0.3 (48%)
	Ser-16	2.2 ± 0.2	0.4 ± 0.1	1.0 ± 0.1 (5%)	–
	Phe-17	1.7 ± 0.4	0.2 ± 0.3	–	–

The degree of insertion of each residue in the membrane is characterized by their insertion depth, which is defined as the center-of-mass distance between the side chain and the membrane, and their solvent accessible surface area (SASA) as shown on the third and fourth columns respectively. For comparison, the upper layer of phosphorous is at 2.0 nm from the center of the membrane. The number of salt-bridges and hydrogen bonds of each residue with the phospholipids are shown on the fifth and sixth columns respectively. The average for these latter two quantities is taken over nonzero values only whose occurrence is shown in parenthesis. Averages are taken over the last 300 ns of each trajectory.

suggesting that this trajectory is not completely trapped (Supporting Information Fig. S10).

We also investigate the dynamics of htt^{NT}Q$_{20}$ insertion starting from a random coil (simulation httNTQ20_coil displayed in Supporting Information Fig. S9). Contrary to what is observed with the peptide without the Q$_N$ segment, nonpolar residues are not found inside the hydrophobic core of the membrane and the peptide adopts rather a random coil globular form. Few structural changes occur during the reorganization step (Supporting Information Fig. S10) because the charged residues and the glutamines interact strongly with the membrane. It is possible that the addition of the Q$_N$ region also increases the conformational entropy of the peptide slowing down significantly the reorganization dynamics that would lead to a structurally ordered partitioning.

As for the htt^{NT} peptide, the noninserted trajectories of htt^{NT}Q$_{20}$ are expected to undergo more structural changes on longer time scales. To investigate the possible conformations for the inserted peptide, a set of three simulations starting from an initially inserted peptide are executed. Two initial configurations are used in which htt^{NT}Q$_{20}$ is either a single α-helix (simulations httNTQ20_α–ins_1 and httNTQ20_α–ins_2) or a α/coil htt^{NT}/Q$_N$ (simulation httNTQ20_α-coil–ins). The average orientation of the htt^{NT} region on the membrane for httNTQ20_α–ins_1 and httNTQ20_α-coil–ins are respectively shown in Figure 7 and Supporting Information Figure S11. Clearly, the single α-helix structure in the htt^{NT} region is stable (Fig. 5). The tilt and rotational pitch angles are also relatively close to the values found for htt^{NT}, although we observe a shift towards smaller tilt and pitch angles with respect to the simulations on htt^{NT} (Table III). These observations do not significantly change when starting from a disordered Q$_N$ region suggesting that its conformation plays a secondary role in

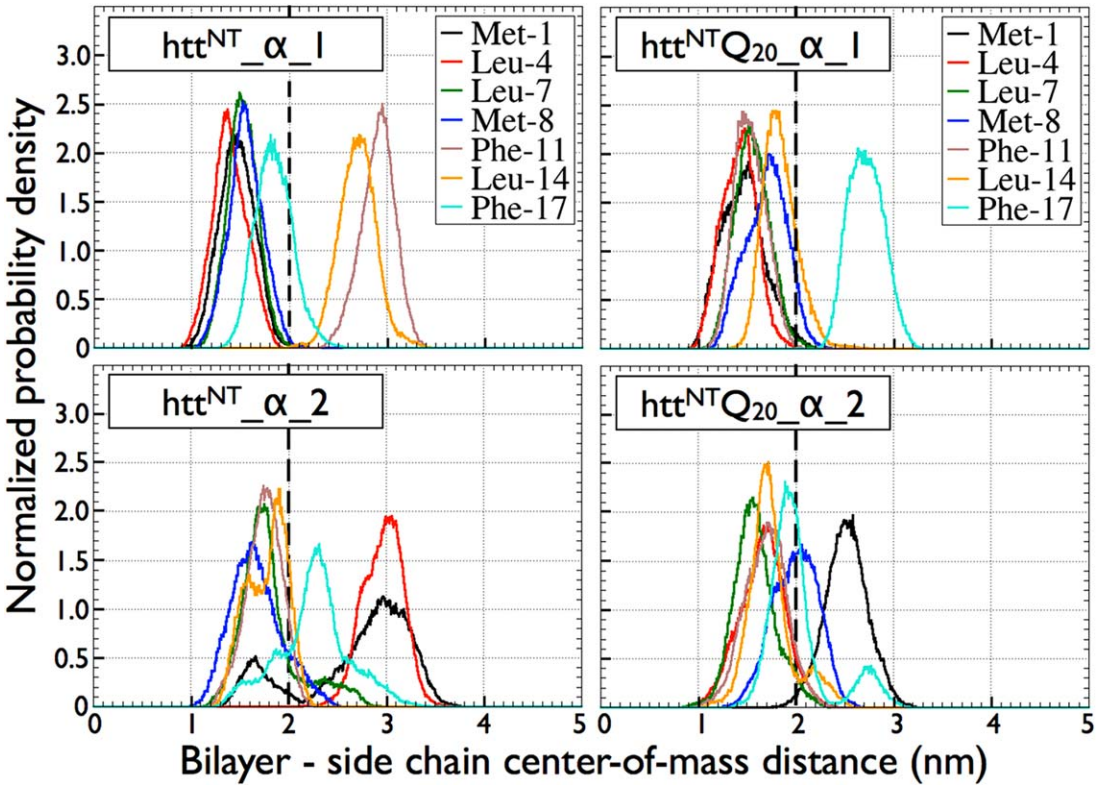

Figure 3

Position probability densities of all nonpolar side-chains with respect to the center-of-mass of the phospholipid bilayer of htt^{NT} for httNT_α_1 and httNT_α_2 (left) and $htt^{NT}Q_{20}$ for httNTQ20_α_1 and httNTQ20_α_2 (right). The average position of the phospholipids' phosphate group is represented by the thick black dotted line near 2.0 Å. The average is taken over the 300–500 ns time interval. [Color figure can be viewed in the online issue, which is available at wileyonlinelibrary.com.]

the structure and orientation of the htt^{NT} region on the bilayer (Fig. 5 and Table III). These similarities between htt^{NT} and $htt^{NT}Q_{20}$ originate from comparable peptide–membrane interactions such as salt-bridges involving mostly Glu-5, Glu-12, Lys-6 and Lys15, hydrogen bonds involving mostly Thr-3 and Ser-13, and burying of nonpolar residues involving mostly Leu-4, Leu-7, Phe-11, and Leu-14 as shown by comparing Tables IV with V. These key interactions seem to be relatively independent of the conformation visited by the Q_N region as seen by comparing Table V with Table VI.

DISCUSSION

The huntingtin protein is related to Huntington's disease through pathways that could involve membrane interactions. Many experimental observations indicate that the huntingtin 17-amino-acid N-terminal (htt^{NT}), positioned just before the polyglutamine segment (Q_N), plays a crucial role in the modulation of its interactions with membrane.[8,9] However, the dynamics and equilibrium properties of its interactions with a phospholipid bilayer as well as the effect of the polyglutamine segment remain mostly unexplained at the atomic level. To our knowledge, no computational study of any sort was designed to look at these aspects to date. The main goal of this study is to fill this gap by investigating the atomic mechanisms responsible for the interactions between the $htt^{NT}Q_N$ peptide and a phospholipid bilayer using molecular dynamics simulations (Table I).

Membrane interactions of htt^{NT}

Interactions of htt^{NT} with phospholipid membranes can lead to perturbations of their physical properties.[29,53,54] Circular dichroism (CD) experiments show that htt^{NT} populates α-helical configurations in hydrophobic environment such as created by the addition of detergents, TFE or unilamellar vesicles in aqueous buffer.[8,23,29] It is believed that, upon binding to the membrane, htt^{NT} becomes α-helical in order to partition its nonpolar amino acids inside the hydrophobic core of the membrane. The resulting structure is expected to be a single α-helix with a well-defined amphipathic plane where the charged amino acids are all placed on the opposite side of the nonpolar amino acids. This

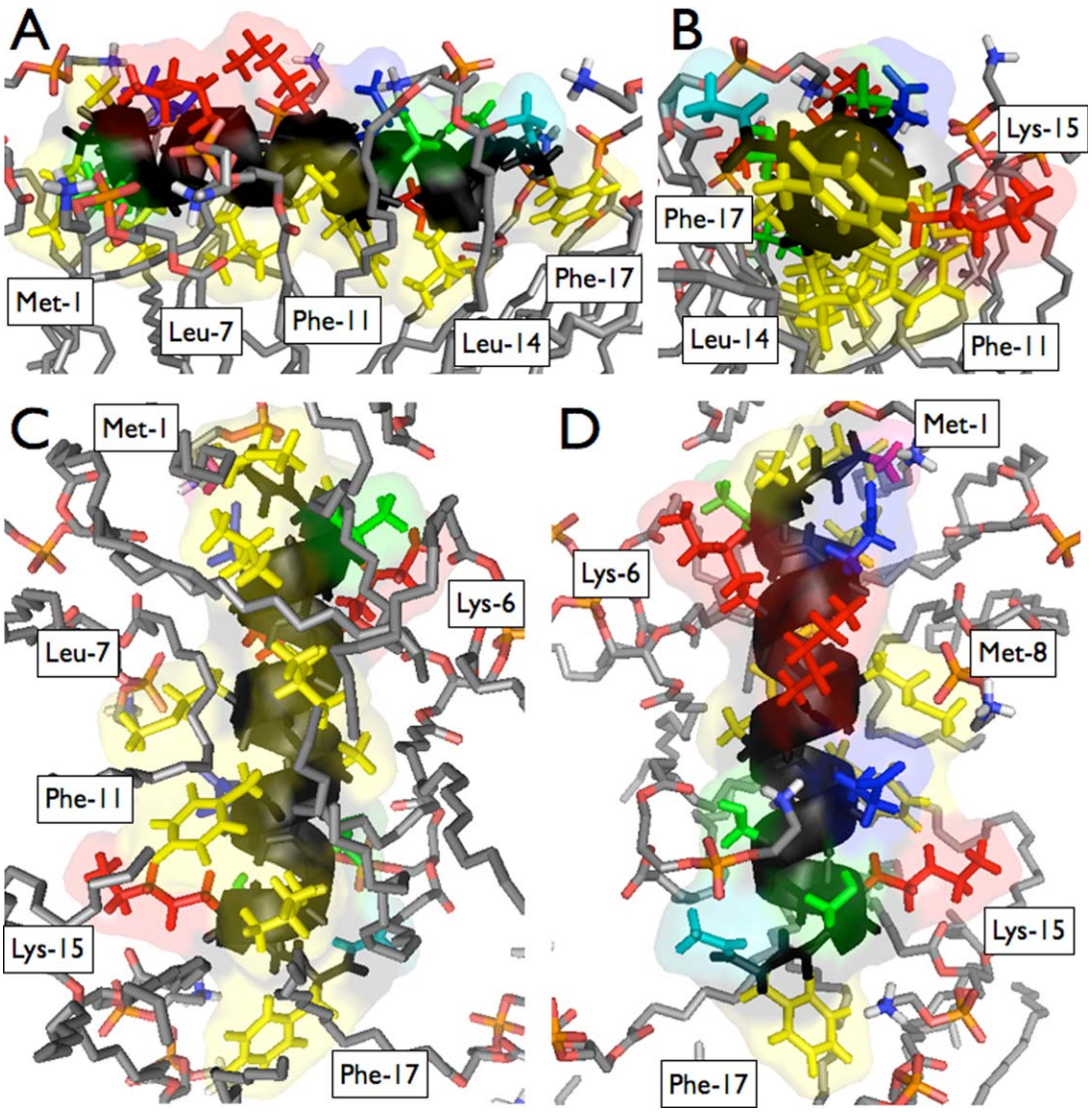

Figure 4

Atomic structure of the average orientation of htt^{NT} over the last 300 ns of httNT_α–ins_1. (**A**) Side view, (**B**) view from the C-terminal, (**C**) view from the membrane, and (**D**) view from the solvent. The nonpolar, negatively charged, positively charged and polar amino acids of the peptide are respectively shown in yellow, red, blue and green. The backbone atoms are displayed in black, and the N- and C-terminal are respectively shown in pink and teal. The phosphorus, oxygen, nitrogen and carbon atoms of the phospholipids are respectively displayed in orange, red, blue and grey. [Color figure can be viewed in the online issue, which is available at wileyonlinelibrary.com.]

hypothesis however lacked atomistic models from either experimental or computational results until now.

In support of this hypothesis, our simulations show indeed that htt^{NT} interacts with the phospholipid bilayer and can partition its nonpolar amino acids inside the hydrophobic core of the membrane (Fig. 1 and fourth column of Table II). Our simulations also show that htt^{NT} can populate α-helical configurations while being adsorbed on or inserted in the membrane in agreement with results from CD experiments[8,23,29] (Fig. 2 and fifth column of Table II). While trajectories httNT_α_2 and httNT_α_3 sample largely random coil–turn configurations, other simulations starting from an initially inserted htt^{NT} (httNT_α–ins_1 and httNT_α–ins_2) lead us to conclude that these are structural intermediates in-route toward the stable α-helical state shown in Figure 4. When compared against our results on the stability of the α-helix in solution (Supporting Information Fig. S3), we observe that the presence of the membrane significantly increases the stability of α-helical configurations for htt^{NT} ($16 \pm 28\%$ in solution vs. $80 \pm 17\%$ in membrane on average), in good agreement with a recent experiment that shows that the α-helical population goes from ∼10% to ∼80% upon stepwise addition of

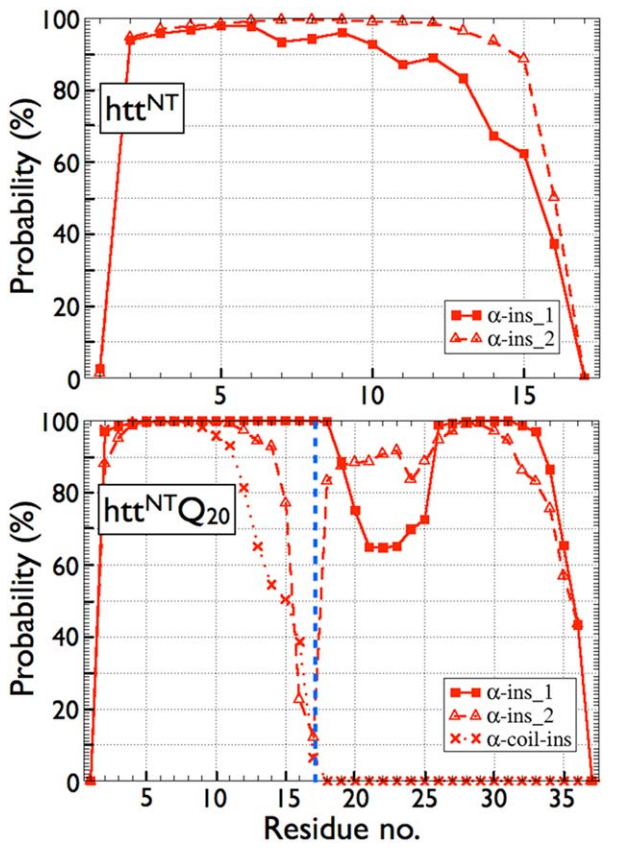

Figure 5

Same as Figure 2, for the simulations starting from an initially inserted peptide for htt^{NT} (httNT_α–ins_1 and httNT_α–ins_2) and htt^{NT}Q$_{20}$ (httNTQ20_α–ins_1, httNTQ20_α–ins_2 and httNTQ20_α-coil–ins). The average is taken over the 200 to 500 ns time interval. [Color figure can be viewed in the online issue, which is available at wileyonlinelibrary.com.]

POPC/POPS (75:25 molar ratio) or POPE/POPG (75:25 molar ratio) vesicles in an aqueous buffer.[29]

Furthermore, our structural results can be compared with the first nuclear magnetic resonance (NMR) atomistic model of htt^{NT} in apolar solution that has been obtained very recently.[97] Showing small variations amongst each other, their twenty atomic models have been obtained by solution NMR in a DPC micellar solution with their orientation discriminated on the basis of solid-state NMR constraints obtained for htt^{NT} on a POPC bilayer. In the following, we compare our results to their model #3, which satisfies best these latter constraints. In their model, htt^{NT} is unstructured from Met-1 to Glu-5 and is an α-helix from Lys-6 to Phe-17. We note however an artifact that could originate from the use of a micellar solution: residues 1 to 3 of the positively charged N-terminal, when their model is oriented as measured experimentally on the phospholipid bilayer, are counterintuitively found directly in the hydrophobic core of the membrane. Instead, our simulations of an initially inserted htt^{NT} on a phospholipid bilayer show, for their part, that the α-helix extends from Ala-2 to Ser-16 (Fig. 5) with the charged N-terminal amine group staying outside the hydrophobic core of the membrane as expected (Fig. 4). In terms of the peptide orientation with respect to the bilayer surface, our structural ensemble populates tilt angles that are near from their measured value of $103 \pm 5^{\circ}$ and rotation pitch angles that are smaller than their measured values of $137 \pm 5^{\circ}$ as shown in Table III. The discrepancy in the rotational pitch angle could be due to a possible dimerization during the NMR experiment resulting in a preferred orientation of the charged residues toward the other peptide, away from the solvent REF 97.

Our results further complement the NMR model by providing a quantitative analysis of the peptide–membrane interactions at the atomic level in terms of insertion depth, surface accessible surface area, hydrogen bonds and salt-bridges (Tables IV–VI). More specifically, this analysis reveals key residues stabilizing the htt^{NT} on the membrane: Glu-5, Glu-12, Lys-6, and Lys-15 are involved in salt-bridges, Thr-3 and Ser-13 are involved in hydrogen bonds, and Leu-4, Leu-7, Phe-11, and Leu-14 are essentially buried. All these residues have been previously recognized to be crucial for the localization, aggregation, and interaction partners of huntingtin N-terminal. For instance, phosphorylation or phosphomimetic mutations of Ser-13 increases its nuclear localization as well as its degradation by the proteasome and lysosome,[98,99] phosphorylation of Thr-3 affect its aggregation reducing the neurotoxicity,[100] SUMOylation of the lysines reduces its ability to form visible SDS-insoluble aggregates,[101] mutations of Leu-4 and Phe-11, which are part of the nuclear export sequence of huntingtin N-terminal along with Leu-7, Leu-14 and Ser-16,[102] to alanines abrogate its ability to target the endoplasmic reticulum,[8] and mutations of Glu-5 and Glu-12 to alanines increase vesicle targeting.[8] Here, our results suggest that mutations and post-transcriptional modifications of these residues, involved in interactions with the membrane, are likely to affect the structure and orientation of the htt^{NT} peptide on the membrane.

As well as providing information on the structural properties of htt^{NT}, our simulations also reveal its insertion dynamics inside a phospholipid bilayer. We observe that it follows, similarly to α-helical membrane-active peptides,[103–105] four main steps: an approach step driven by the charged amino acids of the peptide, a reorganization step during which htt^{NT} undergoes structural changes leading to an anchoring step that can be initiated by either phenalylalanines and an insertion step during which the other nonpolar amino acids are partitioned inside the hydrophobic core of the membrane as reorganization continues (Fig. 1). The details of these steps can vary from one trajectory to the other as to the precise sequence of the residues interacting first with the

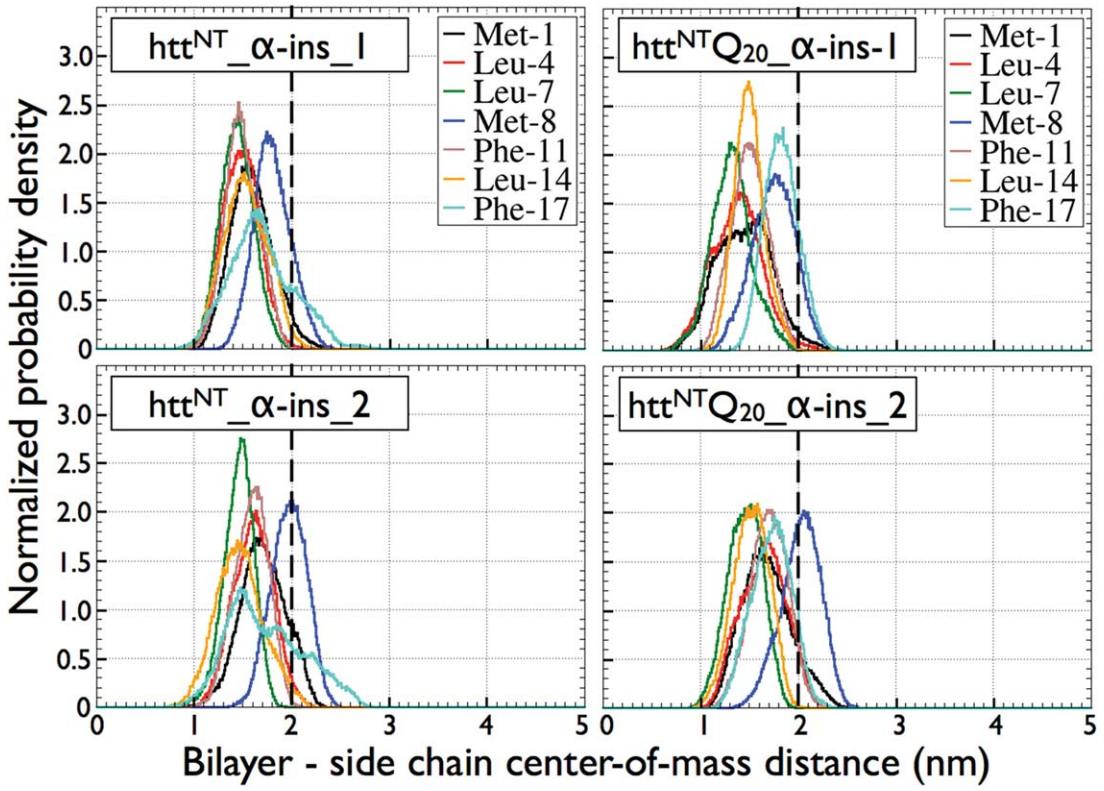

Figure 6

Same as Figure 3, for the simulations starting from an initially inserted peptide for htt^{NT} (httNT_α–ins_1 and httNT_α–ins_2) and htt^{NT}Q$_{20}$ (httNTQ20_α–ins_1 and httNTQ20_α–ins_2). The average is taken over the 200 to 500 ns time interval.

membrane and of the nonpolar residues partitioning (Table II). We also observe that some of the trajectories get trapped for hundreds of nanoseconds between the third and fourth steps waiting for specific conformational events that are necessary for the partitioning of more nonpolar amino acids as well as the formation of the stable α-helix conformation shown in Figure 4. This bottleneck is due to strong electrostatic interactions between the charged amino acids of the peptide and the phospholipids' head group that must be temporarily broken in order for the peptide to proceed toward a more structured and inserted state. As a result, the peptide–membrane Coulomb energy fluctuates considerably as the peptide proceeds towards this state (Supporting Information Fig. S6).

Impact of the glutamines

The number of glutamines in the Q$_N$ region is an important modulator of aggregation and fibrillation in solution as shown from both experiments[19,25] and simulations.[33,39,106] This region also seems to have a role for the membrane interactions of huntingtin.[53,54,56] However, to our knowledge, the atomistic details of the effect of this region on the structure and dynamics of the interactions between htt^{NT}Q$_N$ and a membrane have not been unveiled by experiment or simulation yet.

Our simulations on htt^{NT}Q$_{20}$ show that its insertion dynamics is described by the same four main steps as without the Q$_N$ region: approach, reorganization, anchoring and insertion (Fig. 1). As for htt^{NT}, the details of each step can vary from one simulation to the other (Table II). For instance, the Q$_N$ region is within the first part of the peptide to contact the membrane as can the charged amino acids of the htt^{NT} region. Once adsorbed, the glutamines' side-chain form hydrogen bonds with the phospholipids' head group: 5 ± 2 in httNTQ20_α_1 and 10 ± 3 in httNTQ20_α_2 averaged over the last 200 ns. These interactions between the Q$_N$ region and the membrane provide a stable scaffold for the partitioning of the nonpolar amino acids inside the hydrophobic core of the membrane. As a result, the final configurations of htt^{NT}Q$_{20}$ are more inserted (Fig. 3) and structured (Fig. 2) than htt^{NT}.

Interestingly, the trajectories of htt^{NT} and htt^{NT}Q$_{20}$ starting from an initially inserted α-helical peptide display striking similarities (Fig. 4 vs. Fig. 7). For instance, the htt^{NT} region stays well-structured in a single α-helix starting from Ala^2 (Fig. 5). Also, the position densities of the nonpolar residues inside the hydrophobic core of the

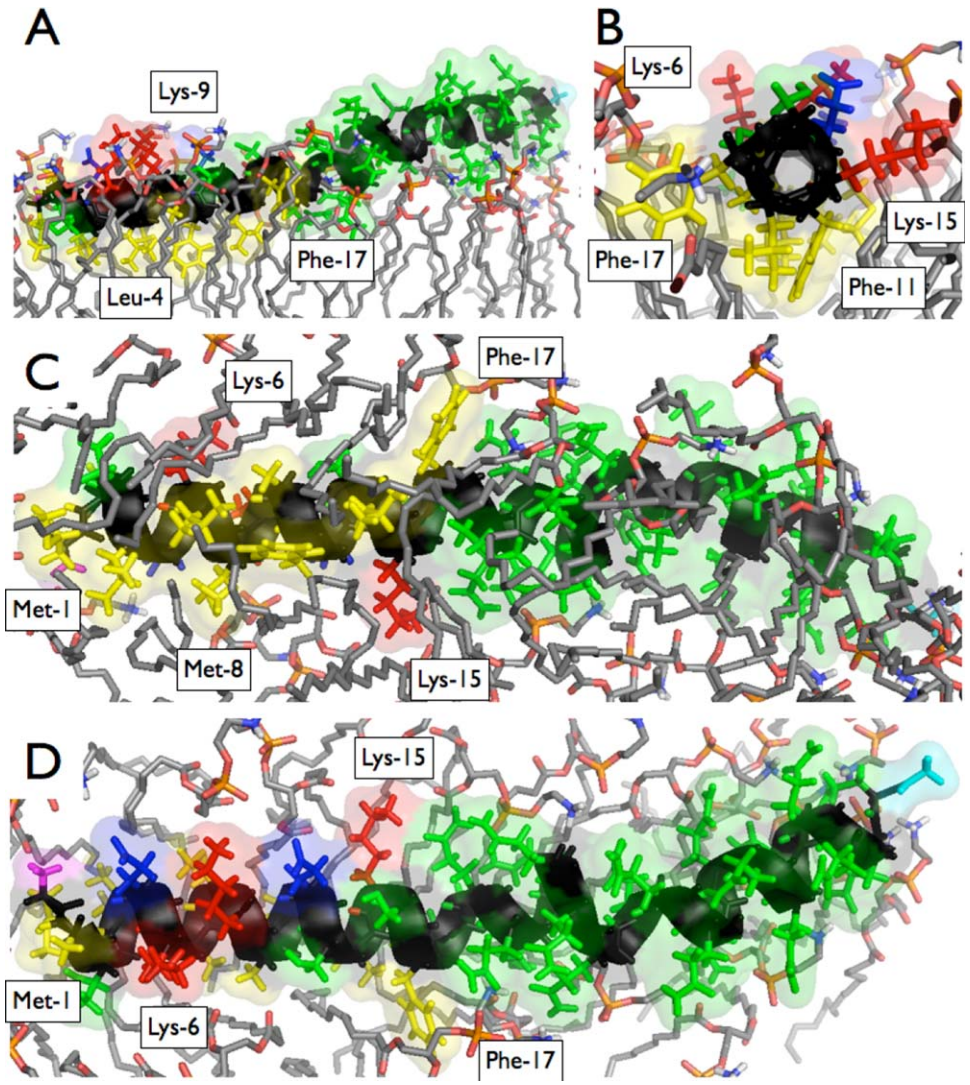

Figure 7

Same as Figure 4, for $htt^{NT}Q_{20}$ (httNTQ20_α–ins_1). [Color figure can be viewed in the online issue, which is available at wileyonlinelibrary.com.]

membrane are similar (Fig. 6). The orientation of the htt^{NT} region is also largely preserved, with a small shift towards smaller tilt and pitch angles (Table III). We observe that these shared features originate from comparable peptide–membrane interactions as seen by comparing Table IV with Table V and are mostly independent of the conformation adopted by the Q_N region (Table VI). Overall, these results suggest that the Q_N region does not significantly modulate the final structure of the htt^{NT} region. Its main role is rather to modulate the insertion dynamics by securing the peptide on the membrane surface through hydrogen bonds. Moreover, as the amyloidogenic Q_N region stays on the surface of the membrane and as it does not interact with the htt^{NT} region (Fig. 7 and Supporting Information Fig. S11, and Tables V and VI), another important role for it could occur during oligomerization by forming extended β-sheet structures with the Q_N region of other $htt^{NT}Q_N$ peptides thus promoting fibrillation. The Q_N regions could be brought in close contact by simple two-dimensional diffusion of the anchored htt^{NT} region on the membrane. The dimer complex could be then further stabilized by the formation of salt-bridges between the charged amino acids of the two htt^{NT} regions.[97] It can then be expected that the membrane, as for other amyloid proteins,[11] could enhance fibrillation of the $htt^{NT}Q_N$ peptide.

Experimental results show that huntingtin and $htt^{NT}Q_N$ interact more strongly with phospholipid membrane as the number of glutamines in Q_N increases.[53,54,56] To investigate this trend, we simulate an intermediate length for the Q_N region: $htt^{NT}Q_{10}$ (simulations httNTQ10_α_1, httNTQ10_α_2, and httNTQ

Table V
Per residue httNT–membrane interactions of $htt^{NT}Q_{20}$ of httNTQ20_α–ins_1 and httNTQ20_α–ins_2

Simulations	Amino acids	Insertion depth (nm)	SASA (nm^2)	H-bonds (no.)	Salt-bridges (no.)
httNTQ20_α–ins_1	$htt^{NT}Q_{20}$	2.2 ± 0.1	14 ± 1	13 ± 3 (100%)	2 ± 1 (90%)
	htt^{NT}	1.8 ± 0.2	4.2 ± 0.7	3 ± 1 (97%)	2 ± 1 (90%)
	Q_{20}	2.5 ± 0.2	10 ± 1	10 ± 3 (100%)	–
	Met-1	1.5 ± 0.3	0.02 ± 0.05	–	–
	Ala-2	2.0 ± 0.3	0.3 ± 0.2	–	–
	Thr-3	1.5 ± 0.3	0.04 ± 0.07	1.0 ± 0.1 (15%)	–
	Leu-4	1.4 ± 0.3	0.01 ± 0.02	–	–
	Glu-5	2.1 ± 0.3	0.6 ± 0.3	1.3 ± 0.5 (54%)	1.1 ± 0.3 (55%)
	Lys-6	2.0 ± 0.3	0.5 ± 0.2	1.4 ± 0.6 (56%)	1.3 ± 0.4 (40%)
	Leu-7	1.3 ± 0.2	0.01 ± 0.01	–	–
	Met-8	1.7 ± 0.2	0.2 ± 0.1	–	–
	Lys-9	2.3 ± 0.2	1.0 ± 0.2	1.0 ± 0.1 (10%)	1.0 ± 0.1 (8%)
	Ala-10	1.7 ± 0.2	0.01 ± 0.01	–	–
	Phe-11	1.5 ± 0.2	0.01 ± 0.03	–	–
	Glu-12	2.2 ± 0.2	0.7 ± 0.2	1.1 ± 0.2 (33%)	1.0 ± 0.2 (34%)
	Ser-13	2.1 ± 0.2	0.1 ± 0.1	1.0 ± 0.2 (33%)	–
	Leu-14	1.5 ± 0.2	0.01 ± 0.01	–	–
	Lys-15	1.9 ± 0.2	0.3 ± 0.2	1.3 ± 0.5 (50%)	1.1 ± 0.3 (34%)
	Ser-16	2.3 ± 0.1	0.4 ± 0.1	1.0 ± 0.1 (7%)	–
	Phe-17	1.8 ± 0.2	0.1 ± 0.1	–	–
httNTQ20_α–ins_2	$htt^{NT}Q_{20}$	2.3 ± 0.1	16 ± 1	14 ± 3 (100%)	2 ± 1 (80%)
	htt^{NT}	1.9 ± 0.2	4.6 ± 0.7	3 ± 2 (93%)	2 ± 1 (80%)
	Q_{20}	2.5 ± 0.2	12 ± 1	11 ± 3 (100%)	–
	Met-1	1.7 ± 0.3	0.05 ± 0.09	–	–
	Ala-2	2.1 ± 0.2	0.2 ± 0.1	–	–
	Thr-3	1.6 ± 0.2	0.03 ± 0.05	1.0 ± 0.1 (14%)	–
	Leu-4	1.6 ± 0.2	0.02 ± 0.05	–	–
	Glu-5	2.3± 0.2	0.9 ± 0.2	1.1 ± 0.2 (12%)	1.0 ± 0.1 (13%)
	Lys-6	2.1 ± 0.2	0.5 ± 0.2	1.3 ± 0.5 (54%)	1.2 ± 0.4 (43%)
	Leu-7	1.5 ± 0.2	0.01 ± 0.01	–	–
	Met-8	2.0 ± 0.2	0.3 ± 0.2	–	–
	Lys-9	2.4 ± 0.2	1.0 ± 0.2	1.0 ± 0.1 (10%)	1.0 ± 0.1 (9%)
	Ala-10	1.7 ± 0.2	0.01 ± 0.02	–	–
	Phe-11	1.7 ± 0.2	0.04 ± 0.06	–	–
	Glu-12	2.4 ± 0.2	0.8 ± 0.2	1.0 ± 0.2 (34%)	1.0 ± 0.1 (35%)
	Ser-13	2.1 ± 0.2	0.1 ± 0.1	1.0 ± 0.2 (45%)	–
	Leu-14	1.5 ± 0.2	0.01 ± 0.01	–	–
	Lys-15	2.0 ± 0.2	0.4 ± 0.2	1.5 ± 0.7 (49%)	1.2 ± 0.4 (38%)
	Ser-16	2.3 ± 0.2	0.2 ± 0.1	1.0 ± 0.1 (8%)	–
	Phe-17	1.7 ± 0.2	0.01 ± 0.01	–	–

Table VI
Per residue httNT–membrane interactions for httNTQ20 of httNTQ20_α-coil–ins

Simulations	Amino acids	Insertion depth (nm)	SASA (nm^2)	H-bonds (no.)	Salt-bridges (no.)
httNTQ20_α-coil–ins	$htt^{NT}Q_{20}$	2.4 ± 0.2	16 ± 2	11 ± 3 (100%)	2±1 (88%)
	htt^{NT}	1.9 ± 0.2	4.6 ± 0.9	3 ± 2 (99%)	2 ± 1 (88%)
	Q_{20}	2.7 ± 0.2	12 ± 1	8 ± 3 (100%)	–
	Met-1	1.7 ± 0.2	0.03 ± 0.08	–	–
	Ala-2	2.2 ± 0.2	0.3 ± 0.1	–	–
	Thr-3	1.6 ± 0.2	0.02 ± 0.03	1.0 ± 0.1 (78%)	–
	Leu-4	1.6 ± 0.2	0.01 ± 0.03	–	–
	Glu-5	2.3 ± 0.2	0.8 ± 0.2	1.1 ± 0.2 (21%)	1.0 ± 0.1 (22%)
	Lys-6	2.1 ± 0.2	0.6 ± 0.2	1.4 ± 0.5 (60%)	1.3 ± 0.4 (53%)
	Leu-7	1.4 ± 0.2	0.1 ± 0.01	–	–
	Met-8	1.9 ± 0.2	0.2 ± 0.2	–	–
	Lys-9	2.4 ± 0.2	0.9 ± 0.2	1.0 ± 0.1 (18%)	1.0 ± 0.1 (17%)
	Ala-10	1.7 ± 0.2	0.01 ± 0.01	–	–
	Phe-11	1.6 ± 0.2	0.02 ± 0.4	–	–
	Glu-12	2.4± 0.2	0.7 ± 0.2	1.1 ± 0.3 (39%)	1.1 ± 0.2 (41%)
	Ser-13	2.0 ± 0.3	0.1 ± 0.1	1.0 ± 0.1 (37%)	–
	Leu-14	1.6 ± 0.2	0.01 ± 0.01	–	–
	Lys-15	2.1 ± 0.2	0.4 ± 0.3	1.1 ± 0.4 (47%)	1.0 ± 0.2 (39%)
	Ser-16	2.3 ± 0.3	0.3 ± 0.2	1.0 ± 0.1 (11%)	–
	Phe-17	1.8 ± 0.3	0.1 ± 0.1	–	–

10_coil). Unfortunately, it becomes rapidly obvious that few clear trends can be extracted between the observations on htt^{NT}, $htt^{NT}Q_{10}$, and $htt^{NT}Q_{20}$ as each system samples very different trajectories on their own (Table II, Fig. 1, and Supporting Information Figs. S5, S9, and S12). We do note however that the approach step of $htt^{NT}Q_{10}$ is very similar to that of $htt^{NT}Q_{20}$ since its glutamines are first to make contact with the membrane. Its trajectories are trapped in the second step due to strong interactions of the glutamines and the charged amino acids with the phospholipids' head group (Supporting Information Fig. S12) as for some trajectories of $htt^{NT}Q_{20}$ (Supporting Information Fig. S9). Finally, our results show that the averaged number of hydrogen bonds between the peptide's side-chains and the membrane for the systems starting from a single α-helix in solution increases from htt^{NT} (3 ± 4 on average) to $htt^{NT}Q_{10}$ (8 ± 3 on average) and to $htt^{NT}Q_{20}$ (12 ± 7 on average). The trajectories of an initially inserted peptide also show this trend: from 3 ± 1 for htt^{NT} to 14 ± 4 for $htt^{NT}Q_{20}$ (on average). The Q_N-length dependence could then originate in part from the increase of the number of hydrogen bonds between the glutamines' side-chain and the phospholipids' head group as the Q_N region gets longer securing more efficiently the N-terminal on the membrane surface.

CONCLUSION

The $htt^{NT}Q_N$ region at the N-terminal of huntingtin is thought to be crucial for huntingtin physiological and pathological roles by modulating its localization to membrane-containing organelles in the cell. The molecular dynamics simulations presented here unveil the structures and dynamics of the interactions between $htt^{NT}Q_N$ and phospholipid membranes at the atomic level. Its insertion dynamics on a membrane is typical of α-helical membrane-active peptides as it follows four main steps—approach, reorganization, anchoring, and insertion—that are very diverse at the atomic level, and it forms a stable α-helix essentially parallel to the surface of the membrane. More specifically to the htt^{NT} peptide, its structure and orientation are not significantly modulated by the presence of the Q_N region whose effects are observed elsewhere. First, it provides a stable scaffold, through hydrogen bonds with the phospholipids' head group, for the partitioning of the nonpolar amino acids of the htt^{NT} region inside the hydrophobic core of the membrane. Second, the Q_N region, being able to form amyloid fibrils in solution, could also promote oligomerization and fibrillation on the membrane by recruiting other $htt^{NT}Q_N$ as our simulations show that it stays accessible to the solvent above the phospholipids' head group. The dimer could then be further stabilized by the formation of salt-bridges between the htt^{NT} regions. Finally, our results complement previous experiments by providing a quantitative analysis of the relationship between the $htt^{NT}Q_N$ peptide and the phospholipid membrane by combining insertion depth, solvent accessible surface area, hydrogen bond and salt-bridge measurements. This analysis reveals the key residues of the htt^{NT} peptide for salt-bridges (Glu-5, Glu-12, Lys-6 and Lys-15), hydrogen bonds (Thr-3 and Ser-13) and nonpolar (Leu-4, Leu-7, Phe-11 and Leu-14) contributions to its stability on the membrane as well as those that are less crucial by staying essentially accessible to the solvent with marginal interactions with the membrane (Lys-9 and Ser-16).

ACKNOWLEDGMENTS

The simulations were executed on the supercomputers of Calcul Québec. The authors thank Evgeniy S. Salnikov and Burkhard Bechinger for helpful discussions.

REFERENCES

1 Bates GP. The molecular genetics of Huntington disease – a history. Nat Rev Genet 2005;6:768–773.
2 Gatchel JR, Zoghbi HY. Diseases of unstable repeat expansion : Mechanisms and common principles. Nat Rev Genet 2005;6:743–755.
3 Orr HT, Zoghbi HY. Trinucleotide repeat disorders. Annu Rev Neurosci 2007;30:575–621.
4 Hands SL, Wyttenbach A. Neurotoxic protein oligomerisation associated with polyglutamine diseases. Acta Neuropathol 2010;120: 419–437.
5 Monoi H, Futaki S, Kugimiya S, Minakata H, Yoshihara K. Poly-L-Glutamine forms cation channels : relevance to the pathogenesis of the polyglutamine diseases. Biophys J 2000;78:2892–2899.
6 Hirakura Y, Azimov R, Azimova R, Kagan BL. Polyglutamine-induced ion channels: a possible mechanism for the neurotoxicity of Huntington and other CAG repeat diseases. J Neurosci Res 2000;60:490–494.
7 Kagan BL, Hirakura Y, Azimov R, Azimova R. The channel hypothesis of Huntington's disease. Brain Res Bull 2001;56:281–284.
8 Atwal RS, Xia J, Pinchev D, Taylor J, Epand RM, Truant R. Huntingtin has a membrane association signal that can modulate huntingtin aggregation, cellular entry and toxicity. Hum Mol Genet 2007;16:2600–2615.
9 Rockabrand E, Slepko N, Pantalone A, Nukala VN, Kazantsev A, Marsh JL, Sullivan PG, Steffan JS, Sensi SL, Thompson LM. The first 17 amino acids of Huntingtin modulate its sub-cellular localization, aggregation and effects on calcium homeostasis. Hum Mol Genet 2007;16:61–77.
10 Lashuel HA, Lansbury PTJ. Are amyloid diseases caused by protein aggregates that mimic bacterial pore-forming toxins? Q Rev Biophys 2006;39:167–201.
11 Lashuel HA, Butterfield SM. Amyloidogenic Protein-Membrane Interactions: Mechanistic Insight from Model Systems. Angew Chem Int Ed 2010;49:5628–5654.
12 Mangiarini L, Sathasivam K, Seller M, Cozens B, Harper A, Hetherington C, Lawton M, Trottier Y, Lehrach H, Davies SW, Bates GP. Exon 1 of the HD gene with an expanded CAG repeat is sufficient to cause a progressive neurological phenotype in transgenic mice. Cell 1996;87:493–506.

13 Zhang QC, Yeh T.-L, Leyva A, Frank LG, Miller J, Kim YE, Langen R, Finkbeiner S, Amzel ML, Ross CA, Poirier MA. A compact b model of huntingtin toxicity. J Biol Chem 2011;286:8188–8196.
14 Nucifora LG, Burke KA, Feng X, Arbez N, Zhu S, Miller J, Yang G, Ratovitski T, Delannoy M, Muchowski PJ, Finkbeiner S, Legleiter J, Ross CA, Poirier MA. Identification of novel potentially toxic oligomers formed in vitro from mammalian-derived expanded huntingtin exon-1 protein. J Biol Chem 2012;287:16017–16028.
15 Ross CA, Poirier MA, Wanker EE, Amzel M. Polyglutamine fibrillogenesis : The pathway unfolds. Proc Natl Acad Sci USA 2003;100: 1–3.
16 Sharma D, Shinchuk LM, Inouye H, Wetzel R, Kirschner DA. Polyglutamine homopolymers having 8 to 45 residues form slablike b-crystallite assemblies. Proteins 2005;61:398–411.
17 Schneider R, Schumacher MC, Mueller H, Nand D, Klaukien V, Heise H, Riedel D, Wolf G, Behrmann E, Raunser S, Seidel R, Engelhard M, Baldus M. Structural characterization of polyglutamine fibrils by solid-state NMR spectroscopy. J Mol Biol 2011; 412:121–136.
18 Wetzel R. Physical chemistry of polyglutamine : Intriguing tales of a monotonous sequence. J Mol Biol 2012;421:466–490.
19 Chen S, Ferrone FA, Wetzel R. Huntington's disease age-of-onset linked to polyglutamine aggregation nucleation. Proc Natl Acad Sci USA 2002;99:11884–11889.
20 Nozaki K, Osamu O, Hiroki T, Shoji T. Amino acids sequences flanking polyglutamine stretches influence their potential for aggregate formation. Neuroreport 2001;12:3357–3364.
21 Robertson AL, Bate MA, Buckle AM, Bottomley SP. The rate of polyQ-mediated aggregation is dramatically affected by the number and location of surrounding domains. J Mol Biol 2011;413:879–887.
22 Kar K, Jayaraman M, Sahoo B, Kodali R, Wetzel R. Critical nucleus size for diseaserelated polyglutamine aggregation is repeat-length dependent. Nat Struct Mol Biol 2011;18:328–337.
23 Thakur AK, Jayaraman M, Mishra R, Thakur M, Chellgren VM, Byeon I.-J.L, Anjum DH, Kodali R, Creamer TP, Conway JF, Gronenborn AM, Wetzel R. Polyglutamine disruption of the huntingtin exon 1 N terminus triggers a complex aggregation mechanism. Nat Struct Mol Biol 2009;16:380–389.
24 Vitalis A, Pappu RV. Assessing the contribution of heterogeneous distributions of oligomers to aggregation mechanisms of polyglutamine peptides. Biophys Chem 2011;159:14–23.
25 Chen S, Berthelier V, Yang W, Wetzel R. Polyglutamine aggregation behaviour in vitro supports a recruitment mechanism of cytotoxicity. J Mol Biol 2001;311:173–182.
26 Liebman SW, Meredith SC. Sticky N17 speeds huntingtin pile-up. Nat Chem Biol 2010;6:7–8.
27 Bhattacharyya A, Thakur AK, Chellgren VM, Thiagarajan G, Williams AD, Chellgren BW, Creamer TP, Wetzel R. Oligoproline effects on polyglutamine conformation of aggregation. J Mol Biol 2006;355:524–535.
28 Darnell G, Orgel JPRO, Pahl R, Meredith SC. Flanking polyproline sequences inhibit b-sheet structure in polyglutamine segments by inducing PPII-like helix structure. J Mol Biol 2007;374:688–704.
29 Michalek M, Salnikov ES, Werten S, Bechinger B. Membrane interactions of the amphipathic amino terminus of huntingtin. Biochem J 2013;52:847–858.
30 Williamson TE, Vitalis A, Crick SL, Pappu RV. Modulation of polyglutamine conformations and dimer formation by the N-terminus of Huntingtin. J Mol Biol 2010;396:1295–1309.
31 Kim MW, Chelliah Y, Kim SW, Otwinowski Z, Bezprozvanny I. Secondary structure of Huntingtin amino-terminal region. Structure 2009;17:1205–1212.
32 Crick SL, Jayaraman M, Frieden C, Wetzel R, Pappu RV. Fluorescence correlation spectroscopy shows that monomeric polyglutamine molecules form collapsed structures in aqueous solutions. Proc Natl Acad Sci USA 2006;103:16764–16769.
33 Vitalis A, Wang X, Pappu RV. Atomistic simulations of the effects of polyglutamine chain length and solvent quality on conformational equilibria and spontaneous homodimerization. J Mol Biol 2008;384:279–297.
34 Vitalis A, Lyle N, Pappu RV. Thermodynamics of b-sheet formation in polyglutamine. Biophys J 2009;97:303–311.
35 Miettinen MS, Knecht V, Monticelli L, Ignatova Z. Assessing polyglutamine conformation in the nucleating event by molecular dynamics simulations. J Phys Chem B 2012;116:10259–10265.
36 Stork M, Giese A, Kretzschmar HA, Tavan P. Molecular dynamics simulations indicate a possible role of parallel b-helices in seeded aggregation of poly-Gln. Biophys J 2005;88:2442–2451.
37 Chopra M, Reddy AS, Abbott NL, de Pablo JJ. Folding of polyglutamine chains. J Chem Phys 2008;129:135102.
38 Khare SD, Ding F, Gwanmesia KNVDN. Molecular origin of polyglutamine aggregation in neurodegenerative diseases. PLoS Comput Biol 2005;1:e30.
39 Marchut AJ, Hall CK. Effects of chain length on the aggregation of model polyglutamine peptides: molecular dynamics simulations. Proteins 2007;66:96–109.
40 Lakhani VV, Ding F, Dokholyan NV. Polyglutamine induced misfolding of Huntingtin Exon1 is modulated by the flanking sequences. PLoS Comput Biol 2010;6:e1000772.
41 Laghaei R, Mousseau N. Spontaneous formation of polyglutamine nanotubes with molecular dynamics simulations. J ChemPhys 2010;132:165102.
42 Nakano M, Watanabe H, Starikov EB, Rothstein SM, Tanaka S. Mutations effects on structural stability of polyglutamine peptides by molecular dynamics simulation. Interdiscip Sci Comput Life Sci 2009;1:21–29.
43 Cote S, Wei G, Mousseau N. All-atom stability and oligomerization simulations of polyglutamine nanotubes with and without the 17-amino-acid N-terminal fragment of the Huntingtin protein. J Phys Chem B 2012;116:12168–12179.
44 Zanuy D, Gunasekaran K, Lesk AM, Nussinov R. Computational study of the fibril organization of polyglutamine repeats reveals a common motif identified in b-helices. J Mol Biol 2006;358:330–345.
45 Esposito L, Paladino A, Pedone C, Vitagliano L. Insights into structure, stability, and toxicity of monomeric and aggregated polyglutamine models form molecular dynamics simulations. Biophys J 2008;94:4031–4040.
46 Ogawa H, Nakano M, Watanabe H, Starikov EB, Rothstein SM, Tanaka S. Molecular dynamics simulation study on the structural stabilities of polyglutamine peptides. Comput Biol Chem 2008;32: 102–110.
47 Kelley NW, Huang X, Tam S, Spiess C, Frydman J, Pande VS. The predicted structure of the headpiece of the Huntingtin protein and its implications on Huntingtin aggregation. J Mol Biol 2009;388: 919–927.
48 Rossetti G, Cossio P, Laio A, Carloni P. Conformations of the Huntingtin N-term in aqueous solution from atomistic simulations. FEBS Lett 2011;585:3086–3089.
49 Dlugosz M, Trylska J. Secondary structures of native and pathogenic huntingtin Nterminal fragments. J Chem Phys B 2011;115: 11597–11608.
50 Davies SW, Turmaine M, Cozens BA, Difiglia M, Sharp AH, Ross CA, Scherzinger E, Wanker EE, Mangiarini L, Bates GP. Formation of neuronal intranuclear inclusions underlies the neurological dysfunction in mice transgenic for HD mutation. Cell 1997;90:537–548.
51 DiFiglia M, Sapp E, Chase KO, Davies SW, Bates GP, Vonsattel JP, Aronin N. Aggregation of huntingtin in neuronal intranuclear inclusions and dystrophic neuritis in brain. Science 1997;277:1990–1993.
52 Benn CL, Landles C, Li H, Strand AD, Woodman B, Sathasivam K, Li SH, Ghazia-Noori S, Hockly E, Faruque SMEA. Contribution of

nuclear and extranuclear polyQ to neurological phenotypes in mouse models of Huntington's disease. Hum Mol Genet 2005;14: 3065–3078.
53 Kegel KB, Schewkunow V, Sapp E, Masso N, Wanker EE, DiFiglia M, Goldmann WH. Polyglutamine expansion in huntingtin increases its insertion into lipid bilayers. Biochem Biophys Res Co. 2009;387:472–475.
54 Burke KA, Hensal KM, Umbaugh CS, Chaibva M, Legleiter J. Huntingtin disrupts lipid bilayers in a polyQ-length dependent manner. Biochim Biophys Acta 2013;1828:1953–1961.
55 Kegel KB, Sapp E, Yoder J, Cuiffo B, Sobin L, Kim YJ, Qin Z-H, Hayden MR, Aronin N, Scott DL, Isenberg G, Goldmann WH, DiFiglia M. Huntingtin associates with acidic phospholipids at the plasma membrane. J Biol Chem 2005;280:36464–36473.
56 Kegel KB, Sapp E, Alexander J, Valencia A, Reeves P, Li X, Masso N, Sobin L, Aronin N, DiFiglia M. Polyglutamine expansion in huntingtin alters its interaction with phospholipids. J Neurochem 2009;110:1585–1597.
57 Jang H, Zheng J, Nussinov R. Models of beta-amyloid ion channels in the membrane suggest that channel formation in the bilayer is a dynamic process. Biophys J 2007;93:1938–1949.
58 Jang H, Teran Arce F, Ramachandran S, Capone R, Lai R, Nussinov R. Structural convergence among diverse, toxic beta-sheet ion channels. J Phys Chem B 2010;114:9445–94451.
59 Zhang Y, Luo Y, Deng Y, Mu Y, Wei G. Structural convergence among diverse, toxic beta-sheet ion channels. PLoS One 2012;7: e38191.
60 Jia Y, Qian Z, Zhang Y, Wei G. Adsorption and orientation of human islet amyloid polypeptide (hIAPP) monomer at anionic lipid bilayer : implications for membranemediated aggregation. Int J Mol Sci 2013;14:6241–6258.
61 Pronk S, Pali S, Schulz R, Larsson P, Bjelkmar P, Apostolov R, Shirts MR, Smith JC, Kasson PM, van der Spoel D, Hess B, Lindahl E. GROMACS 4.5: a highthroughput and highly parallel open source molecular simulation toolkit. Bioinformatics 2013;29: 845–854.
62 Hess B, Kutzner C, van der Spoel D, Lindahl E. GROMACS 4.5: a highthroughput and highly parallel open source molecular simulation toolkit. J Chem Theory Comput 2008;4:435–447.
63 van der Spoel D, Lindahl E, Hess B, Groenhof G, Mark AE, Berendsen HJC. GROMACS: Fast, Flexible and Free. J Comput Chem 2005;26:1701–1719.
64 Berendsen HJC, van der Spoel D, van Drunen R. GROMACS: A message-passing parallel molecular dynamics implementation. Comput Phys Commun 1995;91:43–56.
65 Piana S, Lindorff-Larsen K, Shaw DE. How robust are protein folding simulations with respect to force field parametrization? Biophys J 2011;100:L47–L49.
66 Lindorff-Larsen K, Piana S, Palmo K, Maragakis P, Klepeis JL, Dror RO, Shaw DE. Improved side-chain torsion potentials for the Amber ff99SB protein force field. Proteins 2010;78:1950–1958.
67 Best RB, Hummer G. Optimized molecular dynamics force fields applied to the helix-coil transition of polypeptides. J Phys Chem B 2009;113:9004–9015.
68 Hornak V, Abel R, Okur A, Strockbine B, Roitberg A, Simmerling C. Comparison of multiple amber force fields and development of improved protein backbone parameters. Proteins 2006;65:712–725.
69 Jämbeck JPM, Lyubartsev AP. Derivation and systematic validation of a refined all atom force field for phosphatidylcholine lipids. J Phys Chem B 2012;116:3164–3179.
70 Jämbeck JPM, Lyubartsev AP. An extension and further validation of an all-atomistic force field for biological membrane. J Chem Theory Comput 2012;8:2938–2948.
71 Jämbeck JPM, Lyubartsev AP. Another piece of the membrane puzzle : extending slip ids further. J Chem Theory Comput 2013;9: 774–784.
72 Klauda JB, Venable RM, Freites JA, O'Connor JWO, Tobias DJ, Mondragon-Ramirez C, Vorobyov L, MacKerell AD. Update of the CHARMM all-atom additive force field for lipids: validation on six lipid types. J Phys Chem B 2010;114:7830–7843.
73 Nosé S. A unified formulation of the constant temperature molecular dynamics methods. J Chem Phys 1984;81:511–519.
74 Hoover WG. Canonical dynamics: Equilibrium phase-space distributions. Phys Rev A 1985;31:1695–1697.
75 Parrinello M, Rahman A. Polymorphic transitions in single crystals: A new molecular dynamics method. J Appl Phys 1981;52:7182.
76 Nosé S, Klein ML. Constant pressure molecular dynamics for molecular system. Mol Phys 1983;50;1055–1076.
77 Darden T, York D, Pedersen L. Particle mesh Ewald: An N log(N) method for Ewald sums in large systems. J Chem Phys 1993;98: 10089–10092.
78 Essmann U, Perera L, Berkowitz ML, Darden T, Lee H, Pedersen L. A smooth particle mesh Ewald potential. J Chem Phys 1995;103: 8577–8592.
79 Hess B, Bekker H, Berendsen HJC, Fraaije JGEM. A smooth particle mesh Ewald potential. J Comput Chem 1997;18:1463–1472.
80 Miyamoto S, Kollman PA. SETTLE: An analytical version of the SHAKE and RATTLE algorithm for rigid water models. J Comput Chem 1992;13:952–962.
81 Rand RP, Parsegian VA. Hydration forces between phospholipid bilayers. Biochim Biophys Acta 1989;988:351–376.
82 Schmidt TH, Kandt C. LAMBADA and InflateGRO2: Efficient membrane alignment and insertion of membrane proteins for molecular dynamics simulations. J Chem Inf Model 2012;52:2657–2669.
83 MacKerell JAD, Feig M, Brooks CL, III. Extending the treatment of backbone energetics in protein force fields: limitations of gas-phase quantum mechanics in reproducing protein conformational distributions in molecular dynamics simulations. J Comput Chem 2004; 25:1400–1415.
84 MacKerell JAD, Bashford D, Dunbrack RL, Evanseck JD, Fischer MJEA. All-atom empirical potential for molecular modelling and dynamics studies of proteins. J Phys Chem B 1998;102:3586–3616.
85 Duan Y, Wu CSC, Lee MC, Xiong G, Zhang W, Yang R, Cieplak P, Luo R, Lee T, Caldwell J, Wang J, Kollman P. A point-charge force field for molecular mechanics simulations of proteins based on condensed-phase quantum mechanical calculations. J Comput Chem 2003;24:1999–2012.
86 Kaminski GA, Friesner RA, Tirado-Rives J, Jorgensen WL. Evaluation and reparametrization of the OPLS-AA force field for proteins via comparison with accurate quantum chemical calculations on peptides. J Phys Chem B 2001;105:6474–6487.
87 Jorgensen WL, Maxwell DS, Tirado-Rives J. Development and testing of the OPLS all-atom force field on conformational energetics and properties of organic liquids. J Am Chem Soc 1996;118:11225–11236.
88 Lindorff-Larsen K, Maragakis P, Piana S, Eastwood MP, Dror RO, Shaw DE. Systematic validation of protein force fields against experimental data. PLoS One 2012;7:e32131.
89 Piana S, Lindorff-Larsen K, Shaw DE. Protein folding kinetics and thermodynamics from atomistic simulation. Proc Natl Acad Sci USA 2012;109:17845–17850.
90 Beauchamp KA, Lin Y.-S, Das R, Pande VS. Are protein force fields getting better?. A systematic benchmark on 524 diverse NMR measurements. J Chem Theory Comput 2012;8:1409–1414.
91 Cino E, AvChoy W-Y, Karttunen M. Comparison of secondary structure formation using 10 different force fields in microsecond molecular dynamics simulations. J Chem Theory Comput 2012;8: 2725–2740.
92 Jämbeck JPM, Lyubartsev AP. Exploring the free energy landscape of solutes embedded in lipid bilayers. J Phys Chem Lett 2013;4: 1781–1787.

93 Frishman D, Argos P. Knowledge-Based Protein Secondary Structure Assignment. Proteins 1995;23:566–579.

94 Eisenhaber F, Lijnzaad P, Argos P, Sander C, Scharf M. The Double Cube Lattice Method: Efficient Approaches to Numerical Integration of Surface Area and Volume and to Dot Surface Contouring of Molecular Assemblies. J Comput Chem 1995;16:273–284.

95 Lyubartsev AP, Laaksonen A. MDynaMix - A scalable portable parallel MD simulation package fro arbitrary molecular mixtures. Comput Phys Commun 2000;128:565–589.

96 Barlow DJ, Thornton JM. Ion-pairs in proteins. J Mol Biol 1983; 168:867–885.

97 Michalek M, Salnikov ES, Werten S, Bechinger B. Structure and topology of the huntingtin 1-17 membrane anchor by a combined solution and solid-state NMR approach. Biophys J 2013;105:699–710.

98 Thompson LM, Aiken CT, Kaltenbach LS, Agrawal N, Illes K, Khoshnan A, Martinez-Vincente M, Arrasate M, O'Rourke JG, Khashwji H, Lukacsovich T, Zhu YZ, Lau AL, Massey A, Hayden MR, Zeitlin SO, Finkbeiner S, Green KN, LaFerla FM, Bates G, Huang L, Patterson PH, Lo DC, Cuervo AM, Marsh JL, Steffan JS. IKK phosphorylates huntingtin and targets it for degradation by the proteasome and lysosome. J Cell Biol 2009;187:1083–1099.

99 Gu X, Greiner ER, Mishra R, Kodali R, Osmand A, Finkbeiner S, Steffan JS, Thompson LM, Wetzel R, Yang XW. Serines 13 and 16 are critical determinants of full-length human mutant huntingtin induced disease pathogenesis in HD mice. Neuron 2009;64:828–840.

100 Aiken CT, Steffan JS, Guerrero CM, Khashwji H, Lukacsovich T, Simmons D, Purcell JM, Menhaji K, Zhu Y-Z, Green K, LaFerla F, Huang L, Thompson LM, Marsh JL. Phosphorylation of threonine 3 - Implications for huntingtin aggregation and neurotoxicity. J Biol Chem 2009;284:29427–29436.

101 Steffan JS, Agrawal N, Pallos J, Rockabrand E, Trotman LC, Slepko N, Illes K, Lukacsovich T, Zhu Y-Z, Cattaneo E, Pandolfi PP, Thompson LM, Marsh JL. SUMO modification of huntingtin and Huntington's disease pathology. Science 2004;304:100–104.

102 Zheng Z, Li A, Holmes BB, Marasa JC, Diamond MI. An N-terminal nuclear export signal regulates trafficking and aggregation of huntingtin (Htt) protein exon 1. J Biol Chem 2013;288:6063–6071.

103 Bechinger B. A dynamic view of peptides and proteins in membranes. Cell Mol Life Sci 2008;65:3028–3039.

104 Bechinger B, Aisenbrey C. The polymorphic nature of membrane-active peptides from biophysical and structural investigations. Curr Protein Peptide Sci 2012;13:602–610.

105 Polyansky AA, Chugunov AO, Vassilevski AA, Grishin EV, Efremov RG. Recent advances in computational modelling of alpha-helical membrane-active peptides. Curr Protein Peptide Sci 2012;13:644–657.

106 Barton S, Jacak R, Khare SD, Ding F, Dokholyan NV. The length dependence of the polyQ-mediated protein aggregation. J Biol Chem 2007;282:25487–25492.